Physico-chemical, structural, and adsorption properties of amino-modified starch derivatives for the removal of (in)organic pollutants from aqueous solutions

Nataša Karić, Marija Vukčević, Marina Maletić, Silvana Dimitrijević, Mirjana Ristić, Aleksandra Perić Grujić, Katarina Trivunac

PII: S0141-8130(23)01421-6

DOI: https://doi.org/10.1016/j.ijbiomac.2023.124527

Reference: BIOMAC 124527

To appear in: *International Journal of Biological Macromolecules*

Received date: 28 November 2022

Revised date: 13 April 2023

Accepted date: 16 April 2023

Please cite this article as: N. Karić, M. Vukčević, M. Maletić, et al., Physico-chemical, structural, and adsorption properties of amino-modified starch derivatives for the removal of (in)organic pollutants from aqueous solutions, *International Journal of Biological Macromolecules* (2023), https://doi.org/10.1016/j.ijbiomac.2023.124527

Physico-chemical, structural, and adsorption properties of amino-modified starch derivatives for the removal of (in)organic pollutants from aqueous solutions

Nataša Karić[a, *], Marija Vukčević[b], Marina Maletić[a], Silvana Dimitrijević[c], Mirjana Ristić[b], Aleksandra Perić Grujić[b], Katarina Trivunac[b]

[a] Innovation Center of Faculty of Technology and Metallurgy, Karnegijeva 4, 11120 Belgrade, Serbia

[b] University of Belgrade, Faculty of Technology and Metallurgy, Karnegijeva 4, 11120 Belgrade, Serbia

[c] Mining and Metallurgy Institute Bor, Zeleni bulevar 35, 19210, Bor, Serbia

* Corresponding author: Nataša Karić, Innovation Center of Faculty of Technology and Metallurgy, Karnegijeva 4, 11060 Belgrade, Serbia

E-mail address: nkaric@tmf.bg.ac.rs

Abstract

In this study, an environmentally sustainable process of crystal violet, congo red, methylene blue, brilliant green, Pb^{2+}, Cd^{2+}, and Zn^{2+} ions adsorption from aqueous solutions onto amino-modified starch derivatives was investigated. The degree of substitution, elemental analysis, swelling capacity, solubility, and FTIR, XRD, and SEM techniques were used to characterize the adsorbents. The influence of pH, contact time, temperature, and initial concentration has been studied to optimize the adsorption conditions. The amino-modified starch was the most effective in removing crystal violet (CV) (65.31-80.46%) and Pb^{2+} (67.44-80.33%) within the optimal adsorption conditions (pH 5, 10 mg dm^{-3}, 25 ^{o}C, 180 min). The adsorption of CV

could be described by both Langmuir and Freundlich adsorption isotherms, while the adsorption of Pb^{2+} ions was better described by the Langmuir isotherm. The pseudo-second order model can be used to describe the adsorption kinetics of CV and Pb^{2+} on all tested samples. The thermodynamic study indicated that the adsorption of CV was exothermic, while the Pb^{2+} adsorption was endothermic. The simultaneous removal of CV and Pb^{2+} from the binary mixture has shown their competitive behavior. Thus, the amino-modified starch is a promising eco-friendly adsorbent for the removal of dyes and heavy metals from polluted water.

Keywords: Native macromolecule; Modification; Adsorption

1. Introduction

Population growth, urbanization, rapid industrialization, over-exploitation of water resources, as well as anthropogenic activities at global level in the last few decades have contributed to the deterioration of water quality [1, 2]. The discharge of untreated domestic, commercial, and industrial waste, the discharge of industrial wastewater, and the leaching of agricultural land are among the main sources of water pollution [3]. Water polluted by dyes, heavy metals, nitroarenes, and pesticides is a global major problem.

Synthetic dyes have been widely used in cosmetics, pharmaceutics, plastic, leather, food, paper printing, and textile industries [3, 4]. They usually have complex aromatic molecular structures that make them more stable and resistant to biodegradation and highly resistant to light, temperature, detergents, and microbial attack, and they enter the food chain most often through bioaccumulation in living aquatic organisms [5]. The presence of dyes in a very low concentration in water, even less than 1 mg L^{-1} for some, is highly visible and undesirable [6]. Heavy metal ions have been reported as priority pollutants, due to their high biological toxicity, even at trace concentrations (ppb range to less than 10 ppm). Environmental

pollution and human exposure to heavy metals are the consequences of anthropogenic activities, such as mining and metallurgy, industrial production (electroplating, electronic, nuclear, petroleum combustion, plastics, textiles, microelectronics, wood preservation, and paper processing plants), as well as domestic and agricultural use of metals and metal-containing compounds. Heavy metals enter into the food chain most often through drinking water and crop irrigation [7, 8].

The development of some novel, environmentally friendly approach to wastewater treatment is a major challenge today, especially for the wastewater loaded with toxic and dangerous inorganic and organic compounds. The methods most often used to remove hazardous pollutants from wastewater are ozonation, filtration, oxidation, ion exchange, reverse osmosis, adsorption, flotation, chemical precipitation, flocculation/coagulation, and membrane separation [9, 10]. Among these, adsorption is known to be the most promising method for wastewater treatment and is considered as economically and operationally very effective for removing dyes and heavy metals from contaminated water, especially with the application of low-cost and high-efficiency adsorbents [11, 12].

Polysaccharides are sustainable and environmentally friendly biopolymers that are naturally produced by living organisms. In this regard, starch, cellulose, chitin, chitosan, and lignin are quite significant sustainable and environmentally friendly organic biopolymers. After cellulose, which is the most abundant biopolymer on earth, starch is the second most abundant biopolymer that can have a wide range of applications in environmental protection [13]. Wide industrial application of natural starch is often limited by its structural defects. The presence of a large number of hydroxyl groups in starch provides more reactive sites for chemical modification, based on the introduction of new functional groups into the starch structure. The introduction of specific functional groups (amino, carbonyl, carboxyl, ester, etc.) improves the adsorption capacity of starch towards heavy metal ions and dyes [14]. In

this study, the modification of starch with melamine and amino acids (cysteine and histidine) was investigated. The modification of starch with melamine creates compounds that are insoluble in water, aqueous mineral acids, and organic solvents, which increases their stability and expands the possibility of industrial application. Until now, these compounds were mainly used in the plastics and textile industry, as well as in the surface coating industry [15]. The use of melamine-modified starch as an adsorbent for the removal of pollutants from water has not been reported in the literature. On the other hand, there are several studies in which starch has been modified with amino acids in order to obtain suitable biosorbents [16]. It is proven that natural amino acids with functional groups have a significant impact on the mobility and bioavailability of heavy metals by forming stable complexes with heavy metals [17].

In this study, starch-based adsorbents were synthesized by a simple, efficient, ecologically and economically acceptable method; reactions were run at room temperature, without the use of expensive and toxic chemicals. The modification of starch with melamine, cysteine, and histidine and its application for the adsorption of dyes and heavy metals has not been reported so far. Moreover, the starch modification procedure described in this research is entirely new. Melamine was chosen as a compound rich in nitrogen (66.6%), while amino acids have a lower percentage of nitrogen, but are considered more environmentally friendly and safer to use. Characterization of unmodified and modified starch revealed the influence of modification on structural and surface properties. The obtained amino-modified starch derivatives were tested as adsorbents for the removal of selected dyes (crystal violet - CV, brilliant green - BG, congo red - CR, and methyl orange - MO) and heavy metal ions (Pb^{2+}, Cd^{2+}, and Zn^{2+}) from aqueous solutions. In order to determine the optimal adsorption conditions for efficient removal of selected dyes and heavy metal ions from aqueous media,

the influence of initial pH value, initial concentration, contact time, and temperature was examined.

2. Experimental part

2.1. Materials and methods

Potato starch was purchased from SuperLab, Serbia (loss on drying at 105 °C <10%, sulphored ash <0.5%), while other chemicals were used for starch modification: sodium hypochlorite (>12%, CAS No: 7681-52-9), melamine (2,4,6-triamino-1,3,5-triazine; 99%, CAS No: 108-78-1), L(-)-cysteine ((R)-2-Amino-3-mercaptopropionic acid; ≥97%, CAS No: 52-90-4), L-histidine ((S)-2-amino-3-(4-imidazolyl)propionic acid; ≥98.5%, CAS No: 71-00-1), sodium hydroxide (pellets, ≥97%, CAS No: 1310-73-2), hydrochloric acid (37%, CAS No: 7647-01-0), and acetic acid (glacial, ≥99.7%, CAS No: 64-19-7). Chemicals were used to test adsorption: crystal violet (hexamethyl pararosaniline chloride; CAS No: 548-62-9), congo red benzidinediazo-bis-1-naphthylamine-4-sulfonic acid; CAS No: 573-58-0), methylene blue (methylthioninium chloride; CAS No: 122965-43-9), brilliant green ([4-[[4-(diethylamino)phenyl]-phenylmethylidene]cyclohexa-2,5-dien-1-ylidene]diethylazanium, hydrogen sulfate; CAS No. 633-03-4), Pb^{2+} (solution of $Pb(NO_3)_2$; CAS No: 10099-74-8), Cd^{2+} (solution of $Cd(NO_3)_2$; CAS No: 10325-94-7) and Zn^{2+} (solution of $Zn(CH_3COO)_2$; CAS No: 5970-45-6).

2.2. Material preparation

Starch modification has been performed in a two-step process; in the first stage, the oxidation of starch was carried out, while in the second step, the modification with melamine and amino acids (cysteine and histidine) occurred. Oxidized starch was obtained using sodium hypochlorite according to the procedure previously described [18]. The synthesis of the material with melamine was carried out in a 500 mL beaker, equipped with a stirrer and a

thermometer. Melamine (6 g), distilled water (35 mL), and acetic acid (4 mL) were mixed and heated at 80 °C until the melamine dissolved. Oxidized starch (20 g) was then added and the suspension was stirred continuously for 2 h without further heating, whereby the final temperature of the mixture was about 30 °C. The mixture was then filtered and washed with 20% aqueous acetic acid to remove unreacted melamine. Finally, the filtered material was dispersed in water (200 mL) and, with stirring, neutralized with NaOH solution. The free base was removed by filtration, then the material was washed with water/methanol mixture and acetone several times; finally it was dried at 50-60 °C to constant weight, and grounded to obtain an amorphous white powder. Materials with amino acids were prepared by mixing oxidized starch (20 g) with distilled water (200 mL) in a 500 mL beaker, equipped with a stirrer and thermometer, for 30 min at 40 °C; then the amino acid (2 g) was added to the obtained suspension and stirred at 40 °C for 3 h. Further, the mixture was filtered and washed several times with distilled water and ethanol. The material was dried at 50 °C to constant weight and then ground to obtain a white powder.

2.3. Material characterization

2.3.1. The degree of substitution (DS)

The degree of amine substitution of prepared samples was experimentally determined using the titration method according to the study [19]. Modified starch (0.5 g) was dissolved in 75% v/v ethanol solution and stirred at 60 °C for 30 min. 0.5 M NaOH (25 mL) was added to the mixture and stirred continuously at 60 °C for 15 min and further at room temperature for 72 h. The solution was titrated with 0.5 M HCl solution using phenolphthalein as an indicator. The degree of substitution (DS_{exp}) was calculated according to Eq (1):

$$DS_{exp} = \frac{\left(\frac{162}{1000}\right) \cdot (2 \cdot C_1 \cdot V_1 - C_2 \cdot V_2)}{1 - \left(\frac{M\,(\mathrm{AFG})}{1000}\right) \cdot (2 \cdot C_1 \cdot V_1 - C_2 \cdot V_2)} \quad (1)$$

where C_1 is the concentration of NaOH (mol dm^{-3}), C_2 is the concentration of HCl (mol dm^{-3}), V_1 is the volume of NaOH (dm^3), V_2 is the volume of HCl (dm^3), m is the mass of the sample, 162 is the molar mass of anhydroglucose unit, and M (AFG) is the molecular weight of amine functional group in starch derivatives.

2.3.2. The elemental analysis

The elemental analysis of all examined adsorbents was performed using Flash Smart 2000 CHNS/O Analyzer (Thermo Fisher Scientific).

The degree of substitution (DS_N) of melamine, cysteine, and histidine for amino-modified starch derivatives was calculated from the nitrogen content using Eq (2) [20]:

$$DS_N = \frac{162 \cdot \%N}{14 \cdot 100 - M\,(\mathrm{AFG}) \cdot \%N} \text{ x } 100 \qquad (2)$$

where *%N* is the ratio of nitrogen content, 14.01 is the atom weight of nitrogen, 162 is the molecular weight of an anhydrous glucose unit (AGU) of starch, and M (AFG) is the molecular weight of amine functional group in starch derivatives.

2.3.3. Dynamic viscosity (η)

The viscosity of the solution of native and modified starch (1M NaOH was used as a solvent) was performed using a capillary viscometer (Cannon-Fenske Reverse Flow Viscometer, SI Analytics™ 28540305) according to the earlier described standard procedure [21] with some modifications. 1.0 g of each material was weighed, calculated on a dry basis, and transferred into a wide-mouth bottle; 1M NaOH solution was added to obtain the total weight of the sample and solution of 50 g. The mixture of the sample and solution of NaOH was heated in a water bath at 40 °C, and stirred at 400 rpm using mechanical stirrer until the sample was completely dissolved. Then, the solution was centrifuged to expel any entrapped air bubbles. The viscosity of the sample solution was determined after cooling at room temperature. The dynamic viscosity was calculated using the following Eq (3):

$$\eta = C \cdot t \cdot \rho \quad (3)$$

where C is the constant of the viscometer ($mm^2\ s^{-2}$), t is the time of sample solution flow through viscometer (s), and ρ is the density of sample solution ($g\ mL^{-1}$).

2.3.4. Cold-water swelling capacity (SC) and water solubility (WS)

A measured amount of sample (0.2 g) was placed in a 100 mL beaker and then 20 mL of deionized water was added; mixing was performed by orbital shaker (Sanyo Orbital Shaker, Japan) for 30 min. The resulting suspension was centrifuged at 4250 rpm for 10 min. Supernatant and precipitate were carefully transferred into Petri dishes respectively and dried overnight in an oven at 105 °C. The *SC* and *WS* were calculated using Eq (4) and Eq (5) [22, 23]:

$$SC = W_1/W_0 \quad (4)$$

$$WS = W_2/(W_2+W_0) \quad (5)$$

where W_0 is the weight of the dry material, W_1 is the weight of the swollen sediment, and W_2 is the weight of the dry supernatant.

2.3.5. Fourier-transform infrared (FTIR) spectroscopy

FTIR analysis was used in order to study the structural characteristics of the materials. Analysis was performed using a Nicolet iS10 spectrometer (Thermo Scientific) in the attenuated total reflectance (ATR) mode with a single bounce 45 ° Golden Gate ATR accessory with a diamond crystal, and DTGS detector. FTIR spectra were obtained within a range of 400-4000 cm^{-1} at 4 cm^{-1} resolution with ATR correction.

2.3.6. X-ray diffraction (XRD)

All of the materials were characterized at room temperature by X-ray powder diffraction (XRPD) using an *Ultima IV* Rigaku diffractometer, equipped with $CuK\alpha_{1,2}$ radiations, using a generator voltage (40.0 kV) and a generator current (40.0 mA). The range of 5-40° 2θ was

used for all powders in a continuous scan mode with a scanning step size of 0.02° and at a scan rate of 2° min^{-1}, using D/TeX Ultra high-speed detector. A monocrystalline silicon sample carrier for sample preparation was used.

2.3.7. Scanning electron microscope (SEM)

The morphology of all examined materials was characterized by a scanning electron microscope (SEM). The type of instrument is FE-SEM, TES-CAN Mira3 XMU, operated at 10 eV. Samples were coated with gold in order to reduce the charging effect and improve image quality.

2.4. Adsorption experiments

The investigation of dyes and heavy metal ions adsorption by amino-modified starch was performed in the batch mixing system, at 150 rpm, at room temperature. All adsorption experiments were done in triplicate.

The influence of the initial pH of the solution on the adsorption of dyes (CV, CR, MB, and BG) from a single dye solution was examined by adjusting the pH to 3, 5, 7, and 9, while the other adsorption parameters (adsorbent dose - 0.05 g, initial concentration - 10 mg dm^{-3}, solution volume - 25 mL, and contact time - 180 min) were kept constant.

The adsorption of heavy metals (Pb^{2+}, Cd^{2+}, and Zn^{2+}) from a single metal ion solution was examined at pH 3, 5, and 8, with a constant dose of the adsorbent (0.05 g), initial concentration (10 mg dm^{-3}), and the volume of the solution (25 mL) for 180 min.

The influence of different initial concentrations of a single solution of CV and Pb^{2+} (10, 25, 50, 100, and 250 mg dm^{-3}) on the adsorption efficiency was determined at the constant adsorbent dosage (0.05 g) and the volume of solution (25 mL) at pH 5 during 180 min.

The adsorption kinetics of CV and Pb^{2+} from a single solution at constant adsorbent dosage (0.1 g), solution volume (100 mL), initial concentration (20 mg dm^{-3}), and pH 5 were examined in the interval from 5 to 180 min.

The effect of different temperatures (25, 35, and 45 °C) on the adsorption efficiency from a single solution of CV and Pb^{2+} was determined at a constant adsorbent dosage (0.05 g) and solution volume (25 mL) at pH 5 for 180 min.

The efficiency of CV and Pb^{2+} removal from dye-metal binary mixture at a constant adsorbent dose (0.05 g), initial concentration (10 mg dm^{-3}), and solution volume (25 mL) during 180 min was investigated, as well. Also, the simultaneous removal of Pb^{2+}, Cd^{2+}, and Zn^{2+} ions from the multicomponent mixture was investigated at a constant adsorbent dosage (0.05 g), initial concentration (10 mg dm^{-3}), and solution volume (25 mL) during 180 min.

The concentration of dyes in the aqueous solution was analyzed using a UV-VIS spectrophotometer (Shimadzu 2600) for the visible range at 582, 498, 464, and 630 nm for CV, CR, MO, and BG, respectively. The concentration of heavy metal ions in an aqueous solution after microfiltration was determined using atomic absorption spectroscopy (Pye Unicam SP9, Philips) at 283.3, 228.8, and 213.9 nm for Pb^{2+}, Cd^{2+}, and Zn^{2+}, respectively.

The affinity of the adsorbent for pollutants can be determined by the adsorption capacity and the percentage of pollutants removal from aqueous solutions [24]. The adsorption capacity, q (mg g^{-1}), can be calculated according to Eq (6):

$$q = \left(\frac{C_0 - C_t}{m}\right) \cdot V \tag{6}$$

The removal efficiency (%) of selected pollutants from aqueous solutions, R, was calculated based on the same data according to Eq (7):

$$\%R = \left(\frac{C_0 - C_t}{C_0}\right) \cdot 100 \tag{7}$$

where C_0 and C_t (mg dm^{-3}) are the concentrations of a pollutant at the initial time and after time t (min), V is the volume of solution (cm^3), and m is the amount of the adsorbent (g).

2.4.1. Adsorption isotherm study

Two adsorption isotherm models (Langmuir and Freundlich) were used to evaluate the mechanisms of selected pollutant adsorption onto examined starch samples.

The nonlinear form of the Langmuir model [25] is expressed by Eq (8):

$$q_e = \frac{q_{max} \cdot K \cdot C_e}{1 + K \cdot C_e} \quad (8)$$

where q_e is the equilibrium adsorption capacity of the adsorbent (mg g^{-1}), q_{max} is the maximum adsorption capacity of the adsorbent (mg g^{-1}), and C_e is the equilibrium concentration (mg dm^{-3}). K is the Langmuir isotherm constant which describes the affinity between pollutants and adsorbents. This constant was used to calculate the dimensionless separation factor, K_L as Eq (9):

$$K_L = \frac{1}{1 + K \cdot C_0} \quad (9)$$

where C_0 is the initial adsorbate concentration (mg dm^{-3}). The K_L value indicates the type of isotherm, to be irreversible (K_L= 0), favorable (0 <K_L< 1), linear (K_L= 1), or unfavorable (K_L> 1).

The nonlinear form of the Freundlich model [26] was expressed by Eq (10):

$$q_e = K_f \cdot C_e^{1/n} \quad (10)$$

where q_e is the equilibrium adsorption capacity of the adsorbent (mg g^{-1}), K_F is Freundlich adsorption equilibrium constant which is positively related to the adsorption capacity (dm^3 g^{-1}), C_e is the equilibrium concentration (mg dm^{-3}), and *1/n* is the constant of adsorption intensity and describes surface heterogeneity.

2.4.2. Adsorption kinetic study

The kinetic study provides information about the reaction rate and possible adsorption mechanism, important for the process efficiency. Adsorption is a time-dependent process,

which is especially important when optimizing design parameters [27]. The experimental data were tested using three kinetic models, pseudo-first order [28], pseudo-second order [29], and intra-particle diffusion [30].

Pseudo-first order model:

$$q_t = q_e \cdot (1 - e^{-k_1 \cdot t}) \quad (11)$$

Pseudo-second order model:

$$q_t = q_e - \left(\frac{1}{q_e} - k_2 \cdot t\right)^{-1} \quad (12)$$

Intra-particle model:

$$q_t = k_{id} \cdot t^{1/2} + C \quad (13)$$

where q_t is the amount of pollutant adsorbed at the time t (mg g^{-1}), q_e is the adsorption quantity at equilibrium (mg g^{-1}), k_1 is the pseudo-first-order kinetic rate constant (min^{-1}), k_2 is the pseudo-second-order kinetic rate constant (mg g^{-1} min^{-1}), k_{id} is the intra-particle diffusion rate constant that can be evaluated from the slope of the linear plot of q_t versus $t^{1/2}$ (mg g^{-1} $min^{1/2}$), and constant C is the intercept.

2.4.2. Thermodynamic study

In order to evaluate the influence of temperature on CV and Pb^{2+} adsorption, the adsorption experiments were conducted in a temperature-controlled water bath, at 25, 35, and 45 °C, at constant shaking speed. The thermodynamic parameters of the adsorption process were calculated using Eq (14) and Eq (15) [16]:

$$lnK = \frac{\Delta S}{R} - \frac{\Delta H}{R \cdot T} \quad (14)$$

$$\Delta G = \Delta H - T\Delta S \quad (15)$$

where ΔG is standard Gibbs free energy (kJ mol^{-1}), ΔH is enthalpy (kJ mol^{-1}) and ΔS is entropy changes (J mol^{-1} K^{-1}). The values of ΔH and ΔS were obtained from the slopes and intercepts of lnK vs. the $1/T$ plot, and the values of ΔG were calculated from the corresponding values of ΔH and ΔS following Eq (14).

3. Results and discussion

3.1. Material characterization

3.1.1. Elemental analysis, degree of amine substitution (DS), and dynamic viscosity (η)

The results of the elemental analysis of the samples as well as the results of the determination of the degree of amino substitution and dynamic viscosity are shown in Table 1. The results of the elemental analysis are well correlated with the nitrogen content in each compound used to modify the starch. The highest percentage of nitrogen was determined in the sample with melamine, 5.57%. Although cysteine has a lower content of nitrogen compared to histidine, the larger steric displacements for histidine binding may explain the similar percentage of nitrogen in the samples with cysteine and histidine (3.39 and 3.38%, respectively). Also, the increase in carbon and hydrogen content is consistent with the presence of a side group from the amino component after starch modification.

Table 1. Results of elemental analysis and determination of DS and *η*.

Sample	Element content, %				DS_N	DS_{exp}	*η*, Pa·s
	N	C	H	S			
St	0.37	41.5	6.75	0.51	-	-	1.21 ± 0.06
St-Melamine	5.57	44.5	9.91	-	1.26	1.09 ± 0.05	0.63 ± 0.05
St-Cysteine	3.39	46.9	10.4	2.34	0.55	0.68 ± 0.05	0.74 ± 0.08
St-Histidine	3.80	50.2	11.9	-	0.77	0.67 ± 0.04	0.76 ± 0.06

The degree of substitution calculated from the nitrogen content determined by elemental analysis is in accordance with the DS values obtained by the volumetric method and represents the number of carbonyl groups, which were formed by the oxidation of hydroxyl groups, substituted with amino compounds, melamine, cysteine, and histidine, per α-D-glucopyranosyl unit of starch (the monomeric unit of starch) [31].

The viscosity of the solution of modified starch is significantly decreased in relation to the viscosity of native starch (Table 1), which can be interpreted by the contribution of the starch

structure disintegration during the modification process. Thus, cleavage of the glycosidic linkages produces short linear and branched chains from both crystalline and amorphous regions, which results in reduced viscosity of modified starch [32]. Also, compared to hydroxyl groups, the presence of bulky groups of melamine and amino acids in the structure of modified starch leads to the loss of the granular structure of starch, which causes a decrease of viscosity, especially for melamine modified starch.

3.1.2. FTIR

The FTIR spectra of unmodified and modified starch are shown in Fig. 1a. In the FTIR spectra of all samples, the peaks which appear at around 3238 and 2930 cm^{-1} are attributed to –OH groups and $–CH_2$ stretching vibrations, respectively [33]. The peak at 1640 cm^{-1} is a typical band residing in the spectra of starch, which is attributed to –OH bending vibration originating from adsorbed water molecules [34], and after modification, the intensity of this peak decreases. The absorbance at around 1002 cm^{-1} reflects the –C–O stretching in the starch structure. A peak of weaker intensity at 1712 cm^{-1} in the spectra of modified starch samples can be attributed to –C=O stretching vibrations [33]. The absorption peak at 3415 cm^{-1} in the FT-IR spectrum of St-Melamine is assigned to –NH–, and those at 3470 and 3122 cm^{-1} are assigned to $–NH_2$ stretching vibration, while the peak at 1547 cm^{-1} was attributed to the triazine ring [35]. The absorption peak at 1586 cm^{-1} can be attributed to the presence of the –C=N group in the St-Cysteine structure [19]. The characteristic peak for the structure of pure cysteine appears at 2550 cm^{-1} and originates from the –S–H stretching vibration [36]. In the FTIR spectrum of St-Histidine, the peak at 1482 cm^{-1} corresponds to the bending vibration of the $–NH_2$ group, while the ring vibration appears at 629 cm^{-1} [37]. By comparing the FTIR spectra, the presence of additional peaks on the FTIR spectra of modified samples was determined, which confirmed the successful synthesis of new starch-based materials.

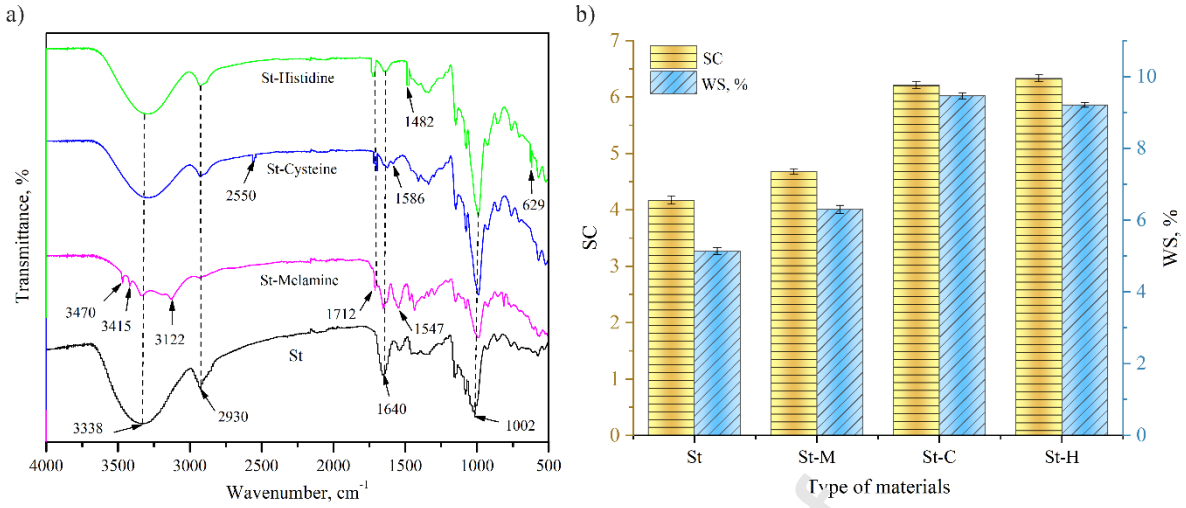

Fig. 1. FTIR spectra (a) and swelling capacity (SC) and water solubility (WS) of samples (b).

3.1.3. Swelling capacity (SC) and water solubility (WS)

The results of swelling capacity (SC) and water solubility (WS) determination are shown in Fig 1b. SC and WS were analysed in a water solution at room temperature, in order to match the adsorption test conditions. A slight increase in SC has been observed for modified materials compared to native starch (4.17), up to 4.68, 6.21, and 6.33 for St-M, St-C, and St-H, respectively. A similar increase in the WS of the modified materials has been observed, 6.30% (St-M), 9.47% (St-C), and 9.21% (St-H) compared to native starch (5.13%). These results can be explained by the introduction of new nitrogen-rich groups that cause a repulsive effect and facilitate water penetration. Partial disruption of the amorphous domain and additional reduction of amylose content may also be the reason for the slight increase of SC and SW of the modified materials compared to natural starch.

3.1.4. XRD

In order to investigate the effect of starch modification on the crystalline structure of materials and changes after adsorption, X-ray diffraction patterns of the dry powders of materials were measured (Fig. 2). Starch is a semi-crystalline macromolecule that contains both crystalline and amorphous domains. The main peaks which indicate crystalline parts in

the starch structure were observed at 2θ = 15.01°, 17.12°, 19.54°, 22.33° and 23.87°. Similar results were reported by Lopez-Rubio et al. 2008 [38], Guo et al. 2020 [39], and Guo et al. 2020b [40] for different types of starch.

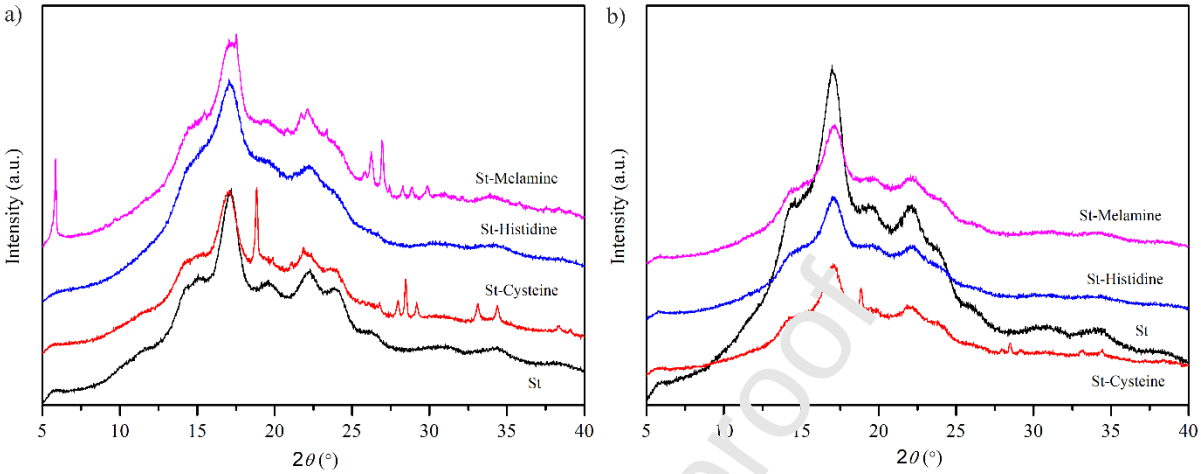

Fig. 2. XRD analysis of St, St-Melamine, St-Cysteine, and St-Histidine before (a) and after adsorption of CV and Pb^{2+} from binary solution (b).

It can be noted that the intensity of the peaks characteristic for the structure of native starch on the XRD patterns of modified starch has been reduced (Fig. 2a), which may be a consequence of the replacement of starch hydroxyl groups with nitrogen-rich groups. The intensity of peaks in the interval from 19.54° to 23.87° has been significantly decreased for St-Histidine, which indicates the reduction of crystalline domains in the starch structure. Additional peaks for St-Melamine at 2θ = 5.97°, 17.52°, 21.34°, and in the range from 25.44° to 30.1° originate from melamine [41]; XRD peaks for St-Cysteine originating from the cysteine structure were observed at 2θ = 18.82° and in the range from 27.95° to 34.38° [42]. XRD patterns of the adsorbents after CV and Pb^{2+} adsorption are shown in Fig. 2b. There is a visible difference in the diffraction patterns before and after the adsorption, in terms of peaks intensity reduction and peaks disappearance, which indicates that functional groups introduced by starch modification are active sites for adsorption. The decrease in the intensity

of peaks and the disappearance of the peaks confirm the loss of crystallinity [43] of the investigated materials after the adsorption of CV and Pb^{2+} from the binary solution.

3.1.5. SEM

The SEM micrographs of the unmodified starch and starch based materials after modification are shown in Fig. 3. It was observed that the surface of the granules of unmodified potato starch is smooth, without pores and cracks, and the granules are mostly oval and spherical (Fig. 3a) [44]. The first stage of starch modification, i.e. oxidation, did not affect the destruction of starch granules, they kept their original shape (Fig. 3b-3d) [45]. In the reaction with melamine, starch was added to the melamine solution at a temperature of 80 °C, resulting in almost complete loss of granules form. The entire surface of the starch granules was covered with parts of melamine in crystalline form (Fig. 3b). Starch modification with amino acids was performed at 40 °C, where gelatinization did not occur, so thermal treatment did not affect the destruction of starch granules (Fig. 3c and 3d). The small agglomeration of particles is observed for both St-Cysteine and St-Histidine. Also, in Fig. 3c, it can be seen that modification with cysteine leads to the deposition of cysteine on the surface of starch granules. On the other hand, modification with histidine (Fig. 3d) leads to the insignificantly changed surface morphology without visible histidine depositions and the assumption of homogenous coating of the starch granules with histidine. The results of the SEM analysis are in complete agreement with the XRD patterns obtained for St, St-Melamine, St-Cysteine, and St-Histidine.

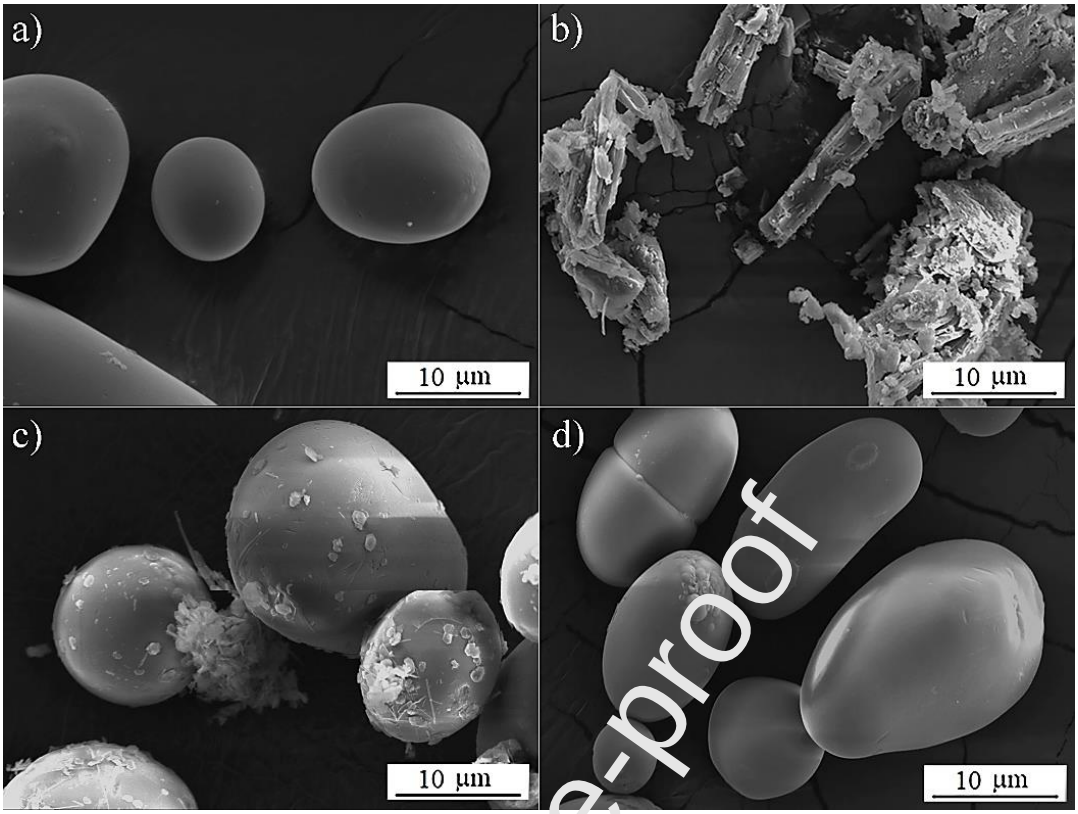

Fig. 3. SEM micrographs of St (a), St-Melamine (b), St-Cysteine (c), and St-Histidine (d).

3.2. Adsorption study

3.2.1 The influence of pH on dyes and heavy metal adsorption

The pH value of the solution is one of the most important factors influencing the adsorption process because it controls the adsorption capacity, and the stability of pollutants, especially dyes. At some pH, dyes are more stable and their removal from aqueous solutions is more difficult, while changing the pH value can lead to a decrease in dyes stability, enabling their easier removal from water. Due to the significant role of the pH value of the solution, the adsorption of dyes (Fig. 4a) and heavy metals (Fig. 4b) from the solution of different initial pH was investigated.

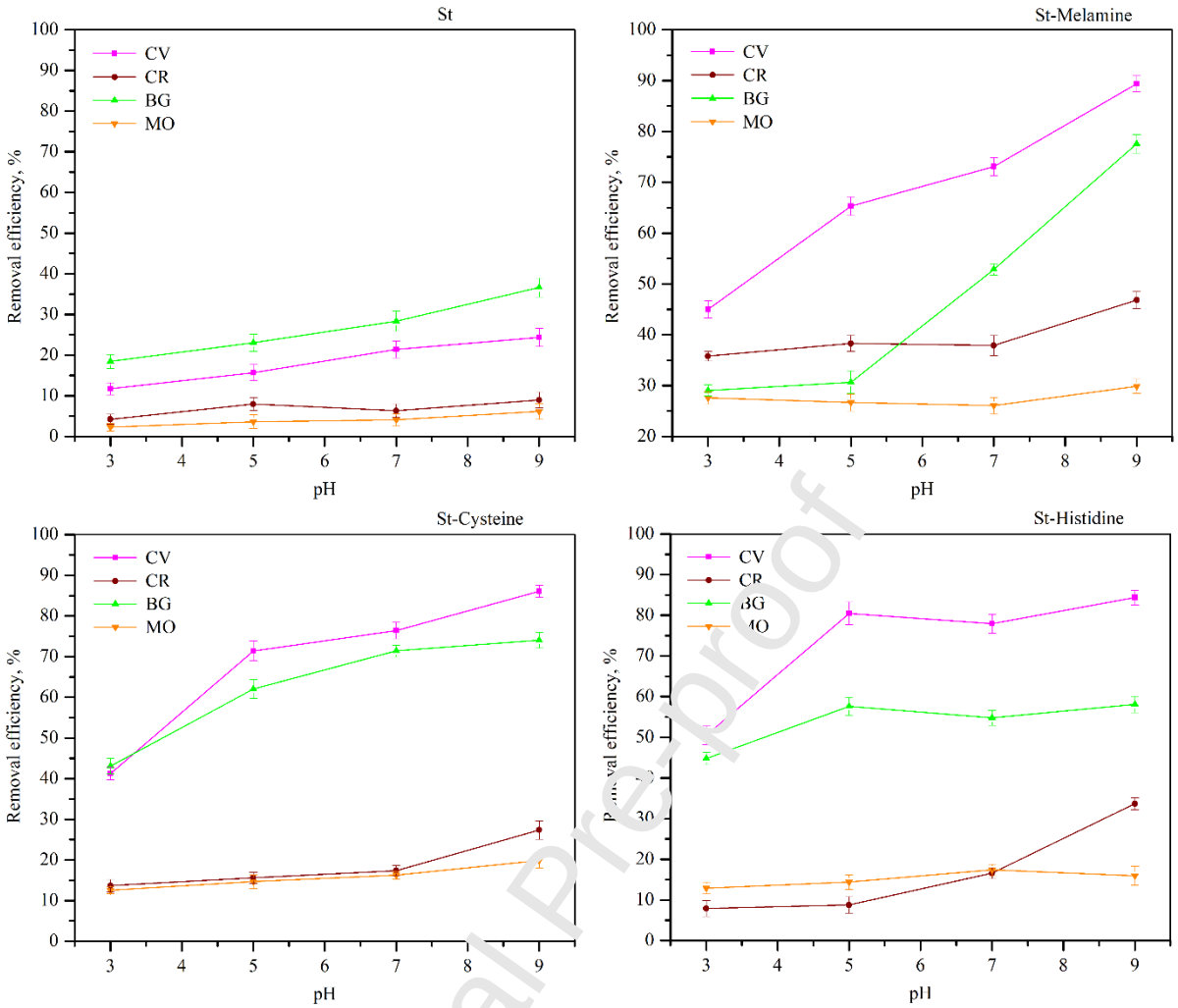

Fig. 4a. Effect of pH solution on the removal efficiency of dyes on St, St-Melamine, St-Cysteine, and St-Histidine at a constant dose of adsorbent (0.05 g), initial concentration (10 mg dm^{-3}), and the volume of the solution (25 mL) during 180 min.

From Fig. 4a, it can be seen that starch modification contributed to an increase in dye removal efficiency compared to unmodified starch. All materials proved effectiveness for cationic dyes, CV and BG removal, while lower efficiency was achieved for anionic dyes, CR and MO. It has been observed that the anionic dye removal by starch modified with melamine was about two times more efficient then the removal by starch modified with cysteine and histidine.

The removal efficiency of CV and BG increases with increasing pH and reaches its maximum at pH 9 for all materials. In a very alkaline solution the conjugate CV structure may be

destroyed due to hydrolysis, and the dye is discoloured [46]. However, all modified starch samples showed the highest efficiency for removing CV in the entire investigated pH range. Therefore, further adsorption experiments were conducted using CV dye, without adjusting the pH of the solution, so that the pH of the material and the solution was in the range 5-6.

A similar trend of increasing removal efficiency with increasing pH was observed for heavy metals, Pb^{2+}, Cd^{2+}, and Zn^{2+} (Fig. 4b).

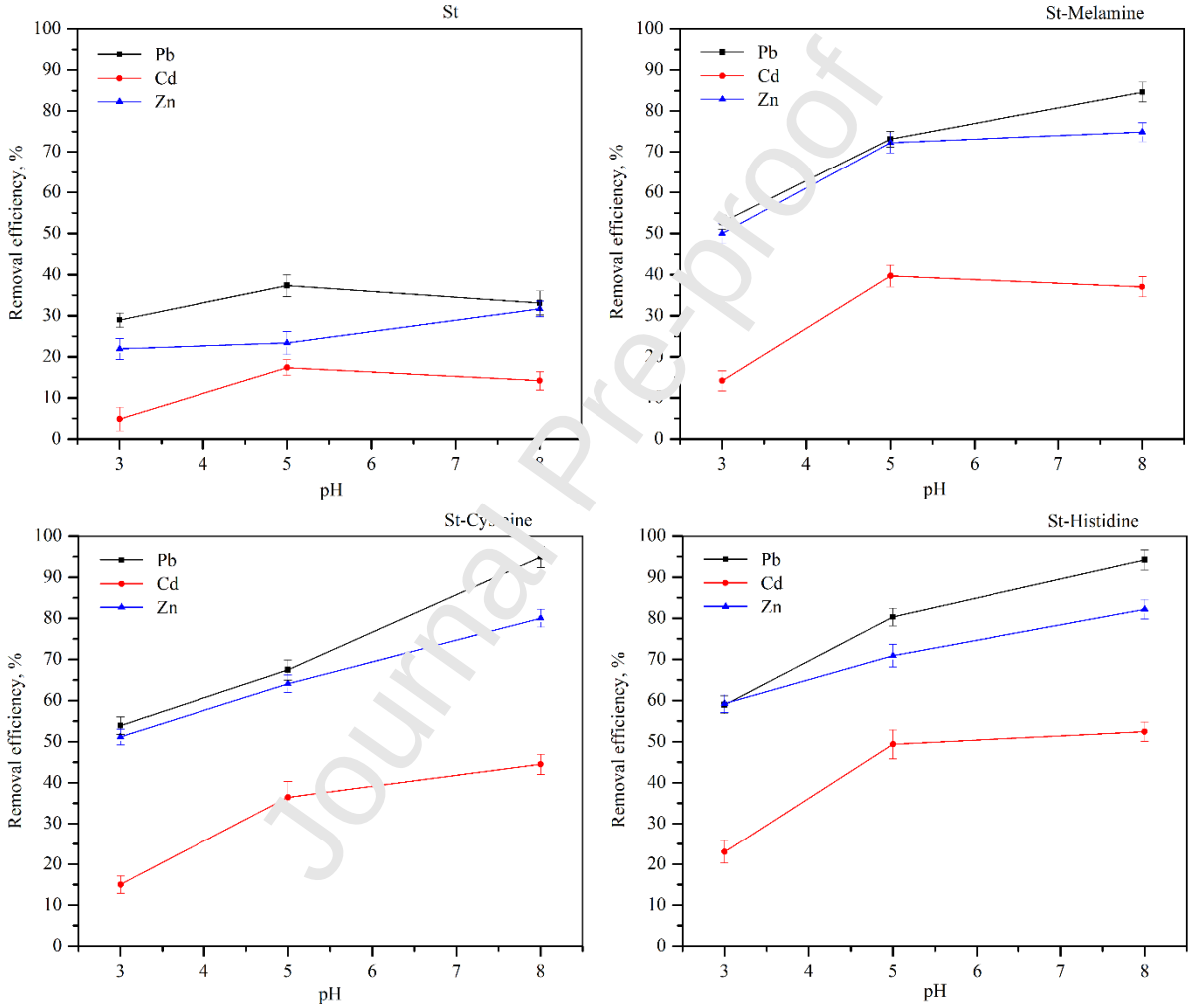

Fig. 4b. Effect of pH solution on the removal efficiency of heavy metal ions on St, St-Melamine, St-Cysteine, and St-Histidine at a constant dose of adsorbent (0.05 g), initial concentration (10 mg dm^{-3}), and the volume of the solution (25 mL) during 180 min.

It was proved that the modification contributed to an increase in the removal efficiency of heavy metal ions compared to unmodified starch. In general, the metal removal trend was

Pb^{2+} > Zn^{2+} > Cd^{2+} for each material (Fig. 4b). The pH of the solution affects the surface charge of the adsorbent, the degree of ionization, and the cation affinity towards surface functional groups. The point of zero charge (pH_{pzc}) of starch, as a basic material was found to be pH 5; the increase in metal removal efficiency with the pH increase can be explained by decreased competition between protons and metal cations for the same functional groups and by the decrease in positive surface charge, which results in a lower electrostatic repulsion between the material surface and the metal ion [47]. High removal efficiency of heavy metal ions (>90% for Pb^{2+}) at pH > 7 (Fig. 4b) can be partly attributed to the chemical precipitation that occurs [48]. In order to reduce the competition between protons and heavy metal cations for surface adsorption sites and, at the same time, to prevent the ion precipitation, all further analyses of metal ions adsorption on starch and amino-modified starch samples were performed without pH adjustment, and the pH of the metal solution with the material was in the range 5-6. At the selected pH, metal ions are dominantly present in the following forms: lead as Pb^{2+}, cadmium as Cd^{2+}, and zinc as Zn^{2+} (Fig. 5).

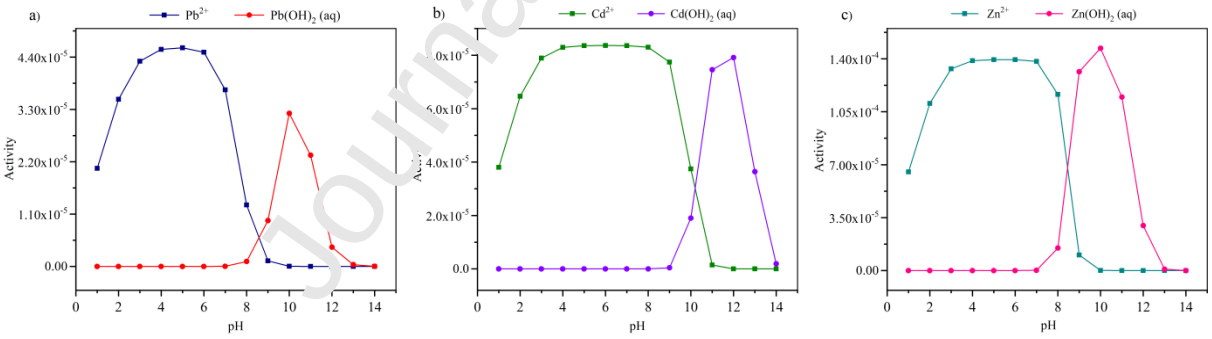

Fig. 5. Speciation of a) Pb^{2+}, b) Cd^{2+}, and c) Zn^{2+}.

3.2.2. The influence of initial concentration on CV and Pb^{2+} adsorption

Wastewater from different industries can contain various concentrations of pollutants, so adsorption studies are carried out at their different initial concentrations. The initial concentration of the pollutant solution can have a significant impact on the efficiency and the adsorption capacity as it provides the necessary driving force to transfer mass between the

aqueous phase (aqueous solution containing the pollutant) and solid phase (adsorbent) [49]. Therefore, the adsorption of CV and Pb^{2+} on modified starch samples (St-Melamine, St-Cysteine, and St-Histidine) was performed with different initial concentrations, ranging from 10 to 250 mg dm^{-3}, while other experimental conditions were kept constant. Fig. 6 shows that the removal efficiency of CV and Pb^{2+} decreases with increasing the initial concentration.

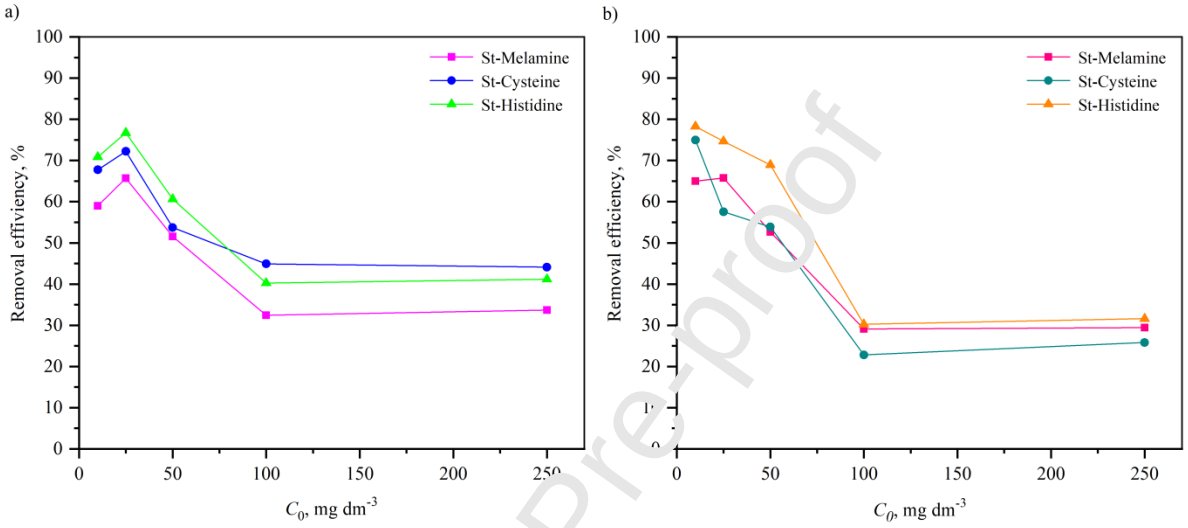

Fig. 6. Effect of initial concentration on the removal efficiency of a) CV and b) Pb^{2+} on St-Melamine, St-Cysteine, and St-Histidine at a constant dose of adsorbent (0.05 g), the volume of the solution (25 mL), during 180 min at pH=5.

When removing CV dye, the removal efficiency increases with the increase of concentration up to 25 mg dm^{-3}; with further concentration increase (up to 100 mg dm^{-3}), the efficiency decreases, and then the plateau has been reached for all materials (Fig. 6a). The similar efficiency trend was observed during Pb^{2+} removal. The highest Pb^{2+} removal efficiency was obtained at initial concentration of 10 mg dm^{-3} for samples St-Cysteine and St-Histidine, and 25 mg dm^{-3} for sample St-Melamine (Fig. 6b). The observed adsorption efficiency decrease at higher dye/metal concentration could be a consequence of adsorbent available active sites saturation, whereby dye molecules and/or metal ions remain in the solution, leading to a decrease in adsorption percentage [50, 51]. On the other hand, adsorption capacity, i.e. the

amount of adsorbed dye and/or metal per unit mass of the adsorbent (mg g^{-1}) increases with increasing initial dye and/or metal concentration (Fig. 7).

3.2.3. Isotherm study

The plots of Langmuir and Freundlich adsorption isotherm are shown in Fig. 7, while parameters and correlation coefficients for adsorption of CV and Pb^{2+} are listed in Table 2.

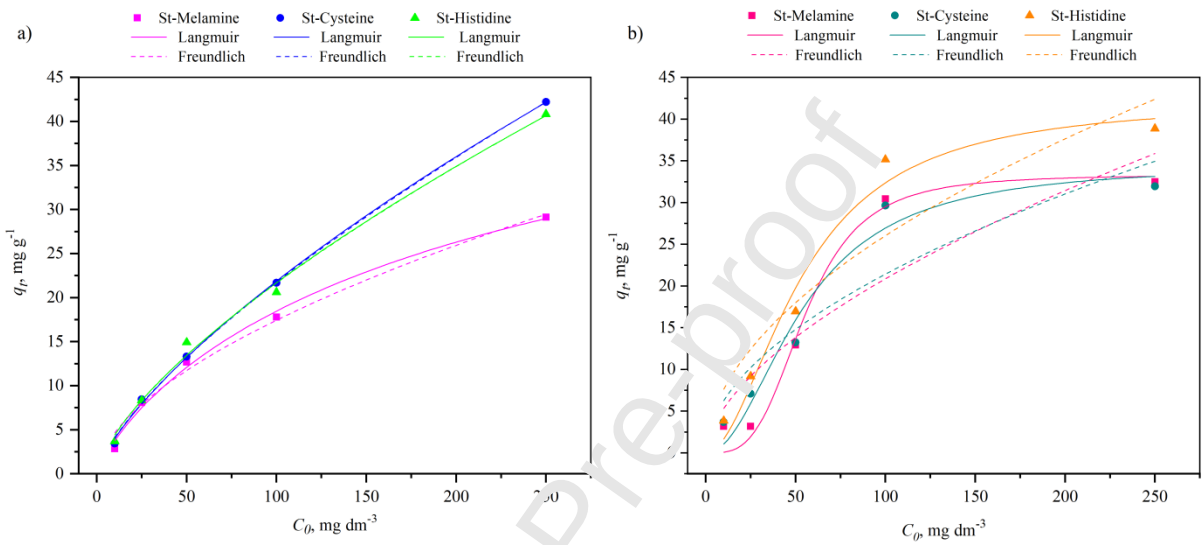

Fig. 7. Nonlinear Langmuir and Freundlich isotherm adsorption models of a) CV and b) Pb^{2+} on St-Melamine, St-Cysteine, and St-Histidine samples.

According to the values of the regression coefficient (R^2) (Table 2), the adsorption of CV on all types of materials can be equally well described by both the Langmuir and Freundlich adsorption isotherm. Although the CV adsorption capacity increased with the initial CV concentration increase, the characteristic plateau was not reached in the examined concentration range. The maximum adsorption capacity of CV dye, calculated from the Langmuir isotherm model, is about four times higher than that of the St-Melamine material and three times of that of St-Cysteine. The adsorption of Pb^{2+} on all materials can be better described by the Langmuir adsorption isotherm (Table 2), when the characteristic plateau is reached at a concentration of 150 mg dm^{-3} for St-Melamine and at 250 mg dm^{-3} for St-Cysteine and St-Histidine. The highest maximum adsorption capacity of Pb^{2+} ions calculated

from the Langmuir isotherm model is for St-Cysteine. This suggests that the adsorption of Pb^{2+} occurs on homogeneously distributed active sites, most likely through the mechanism of physisorption and the ion exchange.

Table 2. Langmuir and Freundlich parameters and correlation coefficients for the adsorption of CV and Pb^{2+} on St-Melamine (St-M), St-Cysteine (St-C), and St-Histidine (St-H) samples.

Material	St-M	St-C	St-H	St-M	St-C	St-H
Pollutant		CV			Pb^{2+}	
Langmuir isotherm						
R^2	0.9899	0.9986	0.9907	0.9681	0.9274	0.9523
q_{max}, mg g^{-1}	58.1748	78.3114	247.625	33.3029	34.5973	42.2049
B	0.012031	0.092291	0.036133	0.08333	0.02844	0.051939
Freundlich isotherm						
R^2	0.9852	0.9991	0.9938	0.7640	0.8109	0.8325
K_f, $mg^{1-1/n}(dm^3)^{1/n}$ g^{-1}	1.24871	0.78048	0.31252	1.36787	1.83193	2.2481
$1/n$	0.57261	0.72279	0.68772	0.53169	0.5341	0.53192

3.2.4. The influence of contact time on CV and Pb^{2+} adsorption

The influence of contact time on CV and Pb^{2+} adsorption was determined in the range from 5 to 180 min. The experimental results are shown in Fig. 8, where it can be seen that the adsorption of CV and Pb^{2+} on all materials increases significantly with increasing contact time up to 60 min, and then the adsorption increases slightly or remains constant for up to 180 min. Likewise, it has been noticed that in the first 30 min of adsorption process is fast due to the high concentration gradient and the availability of a large amount of active sites for the dye adsorption at the beginning of the adsorption process. After 60 min, the adsorption rate decreases as a consequence of the reduction of free sites for the binding of dye molecules on the surface of the adsorbent [52]. A similar dependence of CV and Pb^{2+} adsorption on time has been observed, whereby the materials St-Histidine and St-Cysteine proved to be more effective adsorbents, especially for the removal of Pb^{2+} in a shorter time (Fig. 8).

3.2.5. Kinetic study

The plots of PSO and PFO kinetic models for CV and Pb^{2+} adsorption are given in Figs. 8a and 8b, while the plots of the intra-particle diffusion model for CV and Pb^{2+} adsorption are given in Figs. 8c and 8d, respectively. The kinetic constants and correlation coefficients for adsorption of CV and Pb^{2+} obtained by fitting experimental data with PSO, PFO, and intra-particle diffusion models are shown in Table 3.

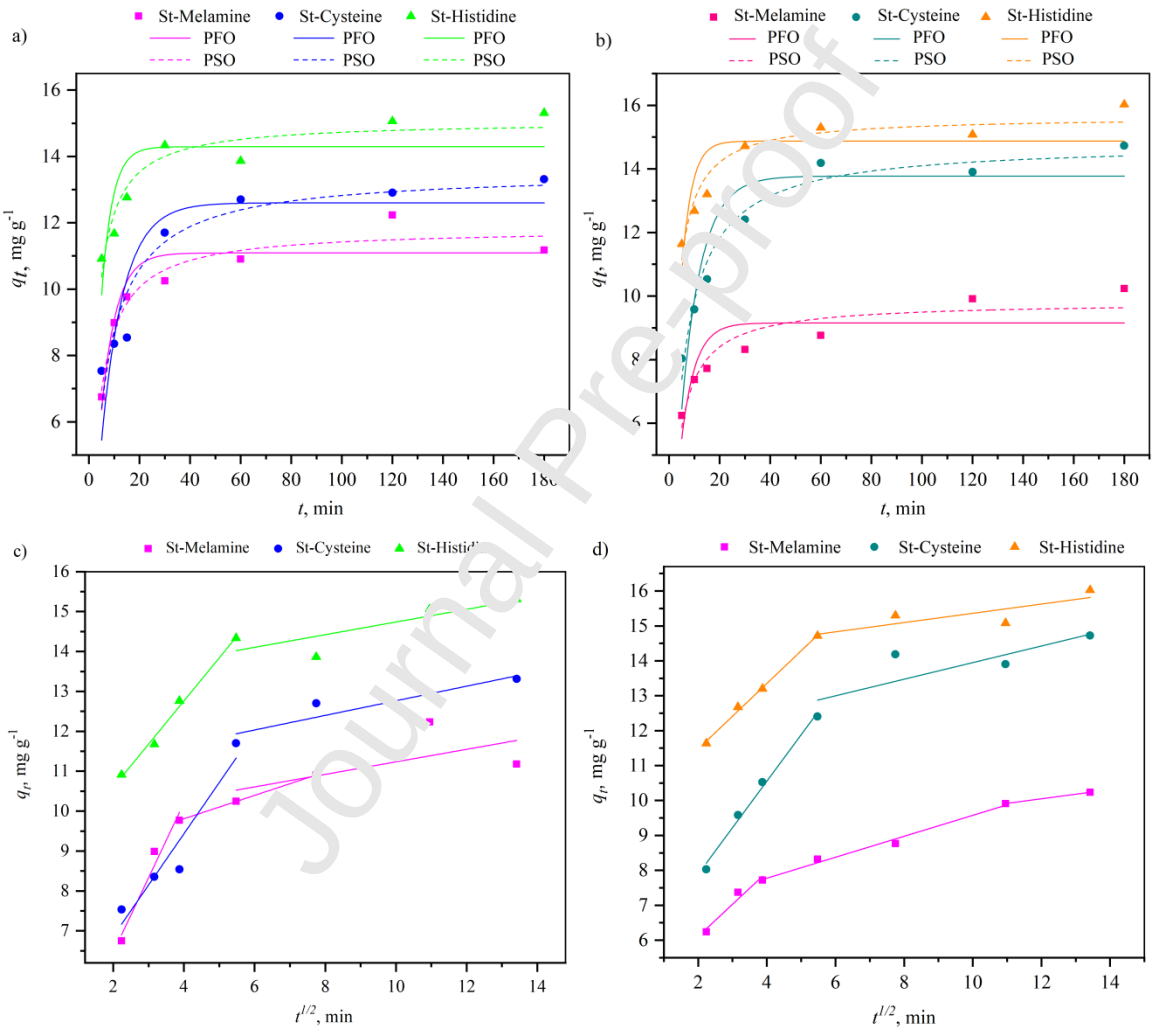

Fig. 8. Pseudo-first order (PFO) and pseudo-second order (PSO) kinetic models of a) CV and b) Pb^{2+} adsorption; and the intra-particle diffusion model of c) CV and d) Pb^{2+} adsorption on St-Melamine, St-Cysteine, and St-Histidine samples.

From the plot of pseudo-first and pseudo-second order kinetic models for CV and Pb^{2+} adsorption (Figs. 8a and 8b) and the comparison of their kinetic parameters (Table 3), the St-Histidine sample proved to be the most effective in removing both pollutants. The adsorption rate and the trend of reaching equilibrium are similar for all materials. The adsorption process was fast, and the equilibrium was reached in approximately 60 min for both pollutants, on all materials. Also, it can be concluded that the pseudo-second order model explains the adsorption kinetics more effectively than the pseudo-first order model, for both pollutants, CV and Pb^{2+}, because it has a higher correlation coefficient (R^2), and better agreement between the calculated and experimental q_e values. This means that the adsorption takes place according to the principle of chemisorption i.e., valence force induced by sharing or exchange of electrons between adsorbate and adsorbent is the rate controlling step of the dye and metal adsorption [53, 54].

Table 3. Kinetic constants and correlation coefficient for adsorption CV and Pb^{2+} on St-Melamine (St-M), St-Cysteine (St-C), and St-Histidine (St-H) samples.

Material	St-M	St-C	St-H	St-M	St-C	St-H
Pollutant		CV			Pb^{2+}	
$q_{e\ exp}$, mg g^{-1}	11.1794	13.3135	15.3100	10.2357	14.7273	16.0265
Pseudo-first order						
R^2	0.8523	0.7298	0.6004	0.6074	0.8130	0.5870
$q_{e\ cal}$, mg g^{-1}	11.09089	12.60122	14.29202	9.15417	13.7732	14.8732
k_1, min^{-1}	0.17039	0.11334	0.23284	0.18470	0.12632	0.25596
Pseudo-second order						
R^2	0.9335	0.8902	0.8895	0.8736	0.9589	0.9119
q_e, mg g^{-1}	11.8232	13.5339	15.0611	9.81356	14.8089	15.6466
k_2, g mg^{-1} min^{-1}	0.024001	0.013314	0.029299	0.030289	0.066336	0.031668
Intra-particle diffusion						
R_1^2	0.9241	0.8805	0.9874	0.90358	0.98735	0.99474
$k_{id,1,}$ mg g^{-1} $min^{1/2}$	1.8722	1.28381	1.08093	0.91841	1.3311	0.93684

C_1, mg g^{-1}	2.71628	4.29823	8.43707	4.27325	5.22875	9.60352
R_2^2	0.9998	0.8031	0.5468	0.98177	0.54864	0.55914
$k_{id,2,}$ mg g^{-1} $min^{1/2}$	0.29274	0.18287	0.15864	0.30017	0.23776	0.13258
C_2, mg g^{-1}	8.63787	10.93639	13.15283	6.57433	11.57175	14.03541
R_3^2	0.16025	-	-	0.88903	-	-
$k_{id,3,}$ mg g^{-1} $min^{1/2}$	0.15693	-	-	0.13110	-	-
C_3, mg g^{-1}	9.6658	-	-	8.47900	-	-

Figs. 8c and 8d have shown the intra-particle model, where the first stage represents the external surface adsorption or instantaneous adsorption stage, the second stage is the gradual adsorption stage, where the intra-particle diffusion is rate-controlled, and the third portion is the final equilibrium stage where the intra-particle diffusion starts to slow down due to extremely low solute concentrations in the solution. The intercept of stage k_{id} gives an idea about the thickness of the boundary layer, i.e., the larger the intercept, the greater the boundary layer effect [55]. Adsorption of both, CV and Pb^{2+} followed the intraparticle diffusion trend. The adsorption process on St-Melamine was characterized by three phases: fast surface adsorption, moderate phase intra-particle diffusion, and a final slow equilibrium phase ($k_{id,1} > k_{id,2} > k_{id,3}$), involving adsorption and desorption within the particle and on the outer surface [56, 57]. The multi-linearity in the intra-particle diffusion diagrams, obtained for St-Melamine adsorption of CV and Pb^{2+}, suggests that the adsorption rate of pollutants can be influenced by the intraparticle diffusion. The highest nitrogen content introduced by melamine modification caused changes in the starch morphology (Fig. 3b) and increased porosity of the surface, making the adsorption on St-Melamine more influenced by intra-particle diffusion. The fact that no phase in the multilinear intra-particle diffusion diagrams passes through the origin suggests that the intra-particle diffusion is not the only rate-controlling step in the overall adsorption process. Adsorption of pollutants on St-Cysteine

and St-Histidine is not influenced by intra-particle diffusion and proceeds through two main phases, rapid surface diffusion, and a final slow equilibrium phase.

3.2.6. Thermodynamic study

The effect of temperature on adsorption efficiency has been examined in the temperature range from 25 to 45 °C. The efficiency of CV adsorption decreased with temperature for all materials (Fig. 9 and Table 4) probably due to the weakening of the physical bonds between the dye molecules and the active sites of the adsorbent; also the increased CV solubility makes the interactions between the dye molecules and water molecules stronger than the interactions between the dye molecules and the adsorbent [47]. Therefore, a temperature of 25 °C was determined as an optimal temperature for CV adsorption, when amino-modified starch is used as an adsorbent, which is very important for the energy efficiency and environmental sustainability of the adsorption process. Thermodynamic parameters (Table 4) have shown that the Δ*G* value for CV adsorption on all tested materials has a negative value, which shows that the adsorption process is spontaneous and possible [52, 54]. Values of *ΔG* between -20 and 0 kJ/mol indicate physisorption, while chemisorption occurs between -80 and -400 kJ/mol [52]. Thermodynamic parameters have shown that the values of *ΔG* obtained for the investigated materials are between -25.8 and -50 kJ/mol, which suggests that both physisorption and chemisorption most likely govern the process of CV adsorption on all materials, which is also consistent with the isotherm study results. The parameter Δ*H* has a negative value, which indicates that the adsorption process is exothermic, while the negative value of Δ*S* indicates that random collisions and irregularities on the surface of the adsorbent are reduced during the CV adsorption process [52].

Table 4. Thermodynamic parameters for adsorption of CV and Pb^{2+} on St-Melamine (St-M), St-Cysteine (St-C), and St-Histidine (St-H) samples.

Samples	Δ*H*, kJ mol^{-1}	Δ*S*, kJ mol^{-1} K^{-1}	Δ*G*, kJ mol^{-1}

	CV	Pb^{2+}	CV	Pb^{2+}	298.15		308.15		318.15	
					CV	Pb^{2+}	CV	Pb^{2+}	CV	Pb^{2+}
St-M	-12.9	7.70	-0.0432	0.0291	-25.8	3.66	-26.3	3.83	-26.7	3.84
St-C	-17.6	18.4	-0.0553	0.0616	-34.1	3.28	-34.7	3.53	-35.2	3.75
St-H	-25.6	25.3	-0.0767	0.0916	-48.5	4.08	-49.3	4.20	-50.0	4.44

The positive values of *ΔG* (Table 4), indicate that the adsorption process of Pb^{2+} on all materials is feasible but nonspontaneous. The positive values of *ΔH* for all the investigated materials suggest that the Pb^{2+} adsorption is an endothermic process, which is supported by the increased adsorption of Pb^{2+} ions with increasing temperature. As the temperature increases, Pb^{2+} ions gain more energy to overcome the energy barrier between metal ions and adsorbents. Simultaneously, on the surface of the adsorbent, additional adsorption sites are created due to the dissociation of the surface groups. The positive value of *ΔS* indicated the increase in the randomness in the system solid/solution interface during the adsorption process of Pb^{2+} [58, 59].

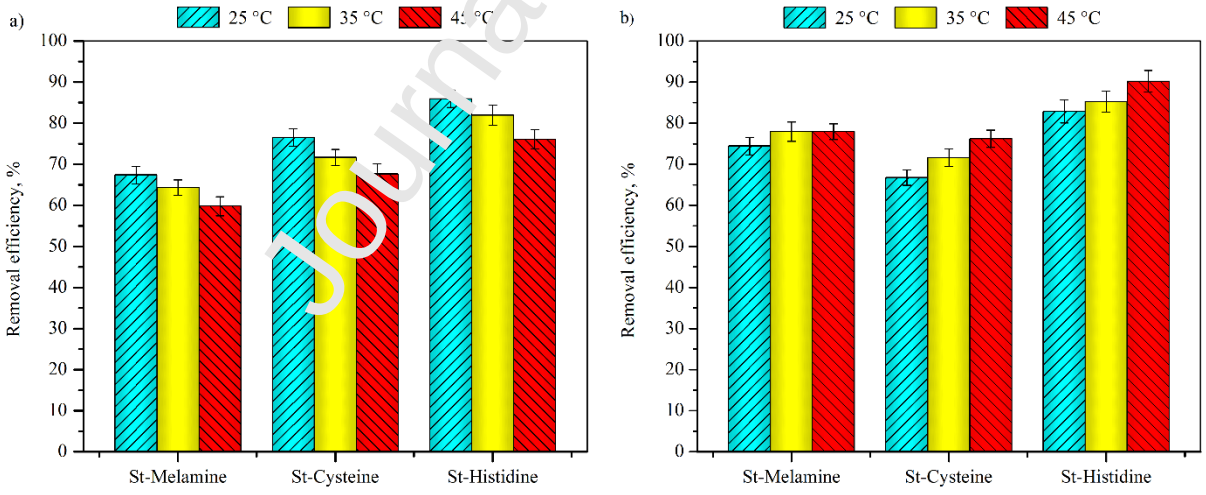

Fig. 9. Effect of temperature on the removal efficiency of CV and Pb^{2+} on St-Melamine, St-Cysteine, and St-Histidine samples.

3.2.7. Adsorption efficiency of simultaneous removal of dye and heavy metals

It is well known that wastewater from many industries can contain mixture of metal ions and organic pollutants, as well as mixture of metal cations. Therefore, in this part of the research, the simultaneous removal of the mixture of CV and Pb^{2+} (Fig. 10a), and the mixture of Pb^{2+}, Cd^{2+}, and Zn^{2+} ions (Fig. 10b) on tested materials has been examined.

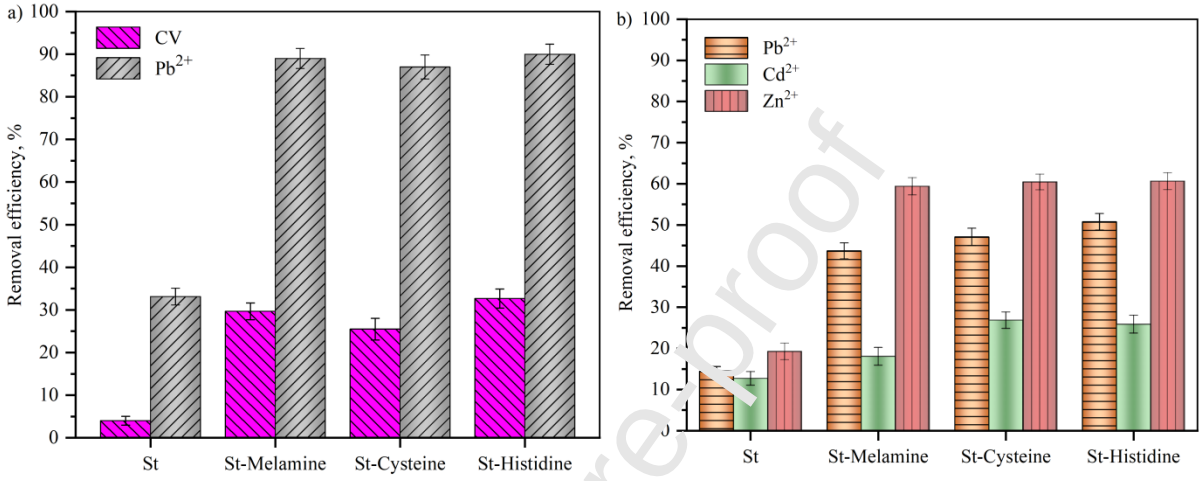

Fig. 10. Results of simultaneous removal of a) CV and Pb^{2+}; b) Pb^{2+}, Cd^{2+}, and Zn^{2+} ions on tested materials.

A multicomponent mixture of pollutants may exhibit three possible types of adsorption effects under competitive conditions: synergism – the effect of the mixture is greater than the individual sorbates in the mixture; antagonism – the effect of the mixture is less than the individual sorbates in the mixture, and no interaction – the mixture has no effect on the adsorption of each sorbate in the mixture [60]. In real conditions, where mixture of pollutants is present and multicomponent adsorption takes place, synergistic adsorption is favourable. The examination of the simultaneous removal of CV and Pb^{2+} from dye-metal binary mixture (Fig. 10a) have shown that their competition for adsorption sites resulted in a decrease in CV removal efficiency and an increase in Pb^{2+} removal efficiency, for all modified materials and unmodified starch. Most likely, Pb^{2+} used to be the first adsorbed on the surface of the adsorbent, and then, the CV dye has been adsorbed on the new layer, with lower efficiency

[61]. The results of the simultaneous removal of metal ions, Pb^{2+}, Cd^{2+}, and Zn^{2+}, from a multi-component mixture (Fig. 10b), indicated a decrease in the removal efficiency compared to the removal efficiency from individual solutions, which was confirmed by most studies related to competitive adsorption of metal ions [62]. Although all three metals are divalent, different properties of these ions in an aqueous solution were responsible for the following binding order of $Zn^{2+} > Pb^{2+} > Cd^{2+}$ ions in a multi-component system. Although Pb^{2+} and Cd^{2+} have larger ionic radii (1.33 A˚ and 0.97 A˚, respectively), they showed lower adsorption properties than Zn^{2+}, which has a smaller ionic radius (0.74 A˚). Therefore, the smaller the ionic radius was, the easier it is for the metal ion to penetrate the boundary layer and adsorb on the surface of the material [63].

3.2.8. Adsorption capacity of various materials – Literature survey

A comparison of the adsorption performances of the starch modified with melamine and amino acids, used in this study, with different adsorbents described in the literature is given in Table 5. In this work, maximum capacities of amino-modified starch for CV and Pb^{2+} adsorption were obtained under following conditions: pH 5, adsorbent mass - 0.05 g, initial pollutant concentration - 10 mg L^{-1}, and equilibrium time - 180 min. In respect to the most of similar studies, the experiments in this work were performed with lower initial concentrations of CV and Pb^{2+} and at room temperature, which provided the closest real conditions for the application of prepared adsorbents. Also, adsorption at a lower temperature ensures the energetic and economic efficiency of the process. Considering the differences in the experimental conditions which influence adsorption capacities, the results obtained in this study are comparable with the literature data, and highly significant due to the natural origin of the starting material and the simple, harmless, and low energy modification process.

Table 5. Maximum adsorption capacities (q_{max}) of various materials on the removal of CV and Pb^{2+} from aqueous solutions.

Target analyte	Type of adsorbent	q_{max}, mg g^{-1}	Reference
CV	Alginate@silver nanoparticles (Alg@AgNPs)	186.93	64
	Alkaline treated sugarcane bagasse	107.5	65
	Guar gum/bentonite bionanocomposite	167.929	66
	Starch Nanoparticle Citrate	833.3	67
	Pectin modified hybrid (Pect/AILP-Kal) nanocomposite	185.24	68
	NaOH-activated *Aerva javanica* leaf powder	315.2	69
	Bio-nanocomposite (Alg-Cst/Kal)	169.49	70
	St-Melamine	58.2	This study
	St-Cysteine	78.3	This study
	St-Histidine	247.6	This study
Pb^{2+}	Guar gum/bentonite bionanocomposite	187.084	66
	Modified cassava starch (MWS/MCS)	370.37/294.12	71
	Chitosan-Iron oxide nanocomposite	214.923	72
	Oxidized corn starch nanoparticles	40.5	73
	Xanthan gum/montmorillonite bionanocomposite	187.08	74
	Papaya peel carbon	40.98	75
	St-Melamine	33.3	This study
	St-Cysteine	34.6	This study
	St-Histidine	42.2	This study

Also, in almost all of the studies presented in Table 5, the importance of desorption and reuse of the adsorbents from an economic and ecological point of view has been indicated.

Regeneration can reduce the need for new adsorbent preparation, as well as the problem of disposal of used adsorbents. It was found that the adsorbents can be successfully reused for CV and Pb^{2+} removal up to the fifth cycle [60, 62, 64, 67, 69, 70]. In order to evaluate the cost-effectiveness and sustainability of the application of amino-modified starch as adsorbents for CV and Pb^{2+} removal in real systems, the focus of our future research will be on the investigation of desorption, regeneration, and the reuse of studied adsorbents.

4. Conclusion

In this study, amino-modified starch was prepared from natural potato starch and nitrogen-rich compounds (amino acids and melamine) and were used as adsorbents for selected dyes and heavy metal ions removal from water. Physico-chemical and structural characterization confirmed the successful incorporation of amino groups into the starch structure. The results have shown that the amino-modified starch was the most effective in removing crystal violet (CV) (65.31-80.46%) and Pb^{2+} (67.44-80.33%), according to the following trend: St-Histidine>St-Cysteine>St-Melamine. After determining the optimal parameters for the CV and Pb^{2+} adsorption, it was concluded that the solution pH, initial concentration, temperature, and contact time were limiting factors for the application of amino-modified starch. Moreover, a significant limiting factor for CV removal from dye-metal binary mixture was the favourable adsorption of Pb^{2+} ions. Relatively fast adsorption of both CV and Pb^{2+} followed the pseudo-second-order kinetics and can be described by Langmuir adsorption isotherm. The intraparticle diffusion affected only the rate of adsorption on St-Melamine, due to changes in starch morphology and increased porosity of the material. Thermodynamic studies showed that CV adsorption was spontaneous and exothermic, while Pb^{2+} adsorption was endothermic. Obtained maximum adsorption capacities (58.2-247.6 mg g^{-1} for CV and 33.3-42.2 mg g^{-1} for Pb^{2+}) have shown that the modification of potato starch without the use

of expensive and toxic chemicals, high temperature and energy consumption can be successfully applied in order to prepare efficient and environmentally friendly adsorbent for their removal from water.

Acknowledgments

This work was financially supported by the Ministry of Education, Science and Technological Development of the Republic of Serbia (Contract No. 451-03-9/2022-14/200135 and 451-03-9/2022-14/200287).

References

[1] M. Danish, T. Ahmad, A review on utilization of wood biomass as a sustainable precursor for activated carbon production and application, Renewable and Sustainable Energy Reviews, 87 (2018) 1–21. https://doi.org/10.1016/j.rser.2018.02.003.

[2] D. Monga, P. Kaur, B. Singh, Microbe mediated remediation of dyes, explosive waste and polyaromatic hydrocarbons, pesticides and pharmaceuticals, Current Research in Microbial Sciences, 3 (2022) 100092. https://doi.org/10.1016/j.crmicr.2021.100092.

[3] H. You, J. Chen, C. Yang, L. Xu, Selective removal of cationic dye from aqueous solution by low-cost adsorbent using phytic acid modified wheat straw, Colloids and Surfaces A: Physicochemical and Engineering Aspects, 509 (2016) 91–98. https://doi.org/10.1016/j.colsurfa.2016.08.085.

[4] R. Ahmad, K. Ansari, Comparative study for adsorption of congo red and methylene blue dye on chitosan modified hybrid nanocomposite, Process Biochemistry, 108 (2021) 90–102. https://doi.org/10.1016/j.procbio.2021.05.013.

[5] R. Kishor, D. Purchase, G.D. Saratale, L.F.R. Ferreira, C.M. Hussain, S.I. Mulla, R.N. Bharagava, Degradation mechanism and toxicity reduction of methyl orange dye by a

newly isolated bacterium Pseudomonas aeruginosa MZ520730, Journal of Water Process Engineering, 43 (2021) 102300. https://doi.org/10.1016/j.jwpe.2021.102300.

[6] C.O. Ademoriyo, C.E. Enyoh, Batch Adsorption Studies of Sunset Yellow and Tartrazine Using Coconut and Groundnut Shells, Journal of Biomedical Research & Environmental Sciences, 6 (2020) 163–172. https://doi.org/10.37871/jbres1138.

[7] P.B. Tchounwou, C.G. Yedjou, A.K. Patlolla, D.J. Sutton, Heavy Metals Toxicity and the Environment, EXS, 101 (2012) 133–164. https://doi.org/10.1007/978-3-7643-8340-4_6.

[8] J. Yang, B. Hou, J. Wang, B. Tian, J. Bi, N. Wang, X. Li, X. Huang. Nanomaterials for the Removal of Heavy Metals from Wastewater. Nanomaterials, 9 (2019) 1–39. https://doi.org/10.3390/nano9030424.

[9] H. Guo, L. Yan, D. Song, K. Li, Citric acid modified Camellia oleifera shell for removal of crystal violet and Pb(II): parameters study and kinetic and thermodynamic profile, Desalination and Water Treatment, 57 (2016) 15373–15383. https://doi.org/10.1080/19443994.2015.1072057.

[10] V. K. Gupta, S. Agarwal, R. Ahmad, A. Mirza, J. Mittal, Sequestration of toxic congo red dye from aqueous solution using ecofriendly guar gum/ activated carbon nanocomposite, International Journal of Biological Macromolecules, 158 (2020) 1310–1318. https://doi.org/10.1016/j.ijbiomac.2020.05.025.

[11] D. Song, K. Pan, A. Tariq, A. Azizullah, F. Sun, Z. Li, Q. Xiong, Adsorptive Removal of Toxic Chromium from Waste-Water Using Wheat Straw and Eupatorium adenophorum, PLoS ONE. 11 (2016) e0167037. https://doi.org/10.1371/journal.pone.0167037.

[12] R. Ahmad, K. Ansari, Chemically treated *Lawsonia inermis* seeds powder (CTLISP): An eco-friendly adsorbent for the removal of brilliant green dye from

aqueous solution, Groundwater for Sustainable Development, 11 (2020) 100417. https://doi.org/10.1016/j.gsd.2020.100417.

[13] M. Nasrollahzadeh, M. Sajjadi, S. Iravani, R.S. Varma, Starch, cellulose, pectin, gum, alginate, chitin and chitosan derived (nano) materials for sustainable water treatment: A review, Carbohydrate Polymers, 251 (2021) 116986. https://doi.org/10.1016/j.carbpol.2020.116986.

[14] M. Haroon, L. Wang, H. Yu, N. M. Abbasi, Z. ul Abdin, M. Saleem, R. U. Khan, R. S. Ullah, Q. Chen, J. Wu, Chemical modification of starch and its application as an adsorbent material, RSC Advances, 6 (2016) 78264-78285. https://doi.org/10.1039/C6RA16795K.

[15] A.S. Giroto, R.H.S. Garcia, L.A. Colnago, A. Klamczynski, G.M. Glenn, C. Ribeiro, Role of urea and melamine as synergic co-plasticizers for starch composites for fertilizer application, International Journal of Biological Macromolecules, 144 (2020) 143–150. https://doi.org/1010.1016/j.ijbiomac.2019.12.094.

[16] J. Li, A. Riley, L. Pu, H. Long, Z. Li, Preparation and Characterization of A Starch-Based Adsorbent for the Effective Removal of Environmental Pollutants Hg (II), Starch - Stärke, 72 (2020) 1900148. https://doi.org/10.1002/star.201900148.

[17] W. Yao, Z. Yang, L. Huang, C. Su, Complexation of Amino Acids with Cadmium and Their Application for Cadmium-Contaminated Soil Remediation, Applied Sciences, 12 (2022) 1114. https://doi.org/10.3390/app12031114.

[18] L.H. Garrido, E. Schnitzler, M.E.B. Zortéa, T.S. Rocha, I.M. Demiate, Physicochemical properties of cassava starch oxidized by sodium hypochlorite, Journal of Food Science and Technology, 51 (2014) 2640–2647. https://doi.org/10.1007/s13197-012-0794-9.

[19] A.A.K.A. Suhai, S.F. Chin, Green Synthesis and Characterization of Amine-Modified Starch Nanoparticles, Starch - Stärke, 73 (2020) 200020. https://doi.org/10.1002/star.202000020.

[20] J. Li, A. Riley, L. Pu, H. Long, Z. Li, Preparation and Characterization of A Starch-Based Adsorbent for the Effective Removal of Environmental Pollutants Hg (II), Starch - Stärke, 72 (2020) 1900148. https://doi.org/10.1002/star.201900148.

[21] Harmonized standards, Methylcellulose, https://www.usp.org/sites/default/files/usp/document/harmonization/excipients/methylcellulose.pdf (accessed 03 March 2023).

[22] C. Fang, J. Huang, Q. Jang, H. Pu, S. Liu, Z. Zhu, Adsorption capacity and cold-water solubility of honeycomb-like potato starch granule, International Journal of Biological Macromolecules, 147 (2020) 741–749. https://doi.org/10.1016/j.ijbiomac.2020.01.224.

[23] J. Zhou, J. Tong, X. Su, L. Ren, Hydrophobic starch nanocrystals preparations through crosslinking modification using citric acid, International Journal of Biological Macromolecules, 91 (2016) 1186–1193. https://doi.org/10.1016/j.ijbiomac.2016.06.082

[24] Q. Lin, K. Wang, M. Cao, Y. Bai, L. Chen, H. Ma, Effectively removal of cationic and anionic dyes by pH-sensitive amphoteric adsorbent derived from agricultural waste-wheat straw, Journal of Taiwan Institute of Chemical Engineers, 76 (2017) 65–72. https://doi.org/10.1016/j.jtice.2017.04.010.

[25] I. Langmuir, The adsorption of gases on plane surfaces of glass, mica and platinum, Journal of the American Chemical Society, 40 (1918) 1361–1403. https://doi.org/10.1021/ja02242a004.

[26] H. Freundlich, Adsorption in solutions, Journal of Physical Chemistry, 57 (1906) 384–410.

[27] K.M. Mousa, A.H. Taha, Adsorption of Reactive Blue Dye onto Natural and Modified Wheat Straw, Journal of Chemical Engineering & Process Technology, 6 (2015) 1000260. https://doi.org/10.4172/2157-7048.1000260.

[28] S. Lagergren, Zur theorieder sogennanten adsorption geloester stoffe, Kungliga Svenska Vetenskapsakademiens. Handlingar, 24 (1908) 1–39, 1908. https://doi.org/10.1007/BF01501332.

[29] Y.S. Ho, G. Mckay, Pseudo-second order model for sorption processes, Process Biochemistry, 34 (1999) 451-465. https://doi.org/10.1016/S0032-9592(98)00112-5.

[30] C. Aharoni, M. Ungarish, Kinetics of activated chemisorption. Part 1.—The non-elovichian part of the isotherm, Journal of Chemical Society Faraday Transactions, 1 (1976) 265–268. https://doi.org/10.1039/F19767200400.

[31] H. Namazi, E. Abdollahzadeh, Drug nanocarrier based in starch-g-amino acids, BioImpacts, 8 (2018) 99–106. https://doi.org/10.15171/bi.2018.12.

[32] P.V. Hung, N.L. Vien, N.T.L. Phi, Resistant starch improvement of rice starches under a combination of acid and heat-moisture treatments, Food Chemistry, 191 (2016) 67–73. http://dx.doi.org/10.1016/j.foodchem.2015.02.002.

[33] S.L.M. El Halal, R. Colussi, V.Z.Pinto, J. Bartz, M. Radunz, N.L.V.Carreño, A.R.G. Dias, E.R. Zavareze, Structure, morphology and functionality of acetylated and oxidised barley starches, Food Chemistry, 168 (2015) 247–256. https://doi.org/10.1016/j.foodchem.2014.07.046.

[34] M. Emeje, R. Kalita, C. Isimi, A. Buragohain, O. Kunle, S. Ofoefule, Synthesis, Physicochemical Characterization and Functional Properties of an Esterified Starch from an Underutilized Source in Nigeria, Africal Journal of Food, Agriculture, Nutrition and Development, 12 (2012) 7001–7018. https://doi.org/10.18697/ajfand.55.10560.

[35] H. Zhu, S. Xu, Preparation and fire behavior of rigid polyurethane foams synthesized from modified urea–melamine–formaldehyde resins, RSC Advances, 8 (2018) 17879. https://doi.org/10.1039/c8ra01846d.

[36] L. Li, L. Liao, Y. Ding, H. Zeng, Dithizone-etched CdTe nanoparticles-based fluorescence sensor for the off–on detection of cadmium ion in aqueous media, RSC Advances, 7 (2017) 10361. https://doi.org/10.1039/c6ra24971j.

[37] M. Nazir, R. Khattak, M.S. Khan, I.I. Naqvi, Study of the histidine complex of uranium(IV): Synthesis, spectrophotometric, magnetic and electrochemical properties, Bulletin of the Chemical Society of Ethiopia, 34 (2020) 557–569. https://doi.org/10.4314/bcse.v34i3.11.

[38] A. Lopez-Rubio, B.M. Flanagan, E.P. Gilbert, M.J. Gidley, A Novel Approach for Calculating Starch Crystallinity and Its Correlation with Double Helix Content: A Combined XRD and NMR Study, Biopolymers, 89 (2008) 761–768. https://doi.org/10.1002/bip.21005

[39] L. Guo, J. Li, Y. Gui, Y. Zhu, B. Yu, C. Tan, Y. Fang, B. Cui, Porous starches modified with double enzymes: Structure and adsorption properties, International Journal of Biological Macromolecules 164 (2020) 1758–1765. https://doi.org/10.1016/j.ijbiomac.2020.07.323.

[40] L. Guo, J. Li, H. Li, Y. Zhu, B. Cui, The structure property and adsorption capacity of new enzyme-treated potato and sweet potato starches, International Journal of Biological Macromolecules, 144 (2020) 863–873. https://doi.org/10.1016/j.ijbiomac.2019.09.164.

[41] H. Tang, K. Ng, S.S. Chui, C. Che, C. Lam, K. Yuen, T. Siu, L.C. Lan, X. Che, Analysis of Melamine Cyanurate in Urine Using Matrix-Assisted Laser

Desorption/Ionization Mass Spectrometry, Analytical Chemistry, 81 (2009) 3676–3682. https://doi.org/10.1021/ac802752n.

[42] M. Ejgenberg, Y. Mastai, Biomimetic Crystallization of L-Cystine Hierarchical Structures, Crystal Growth & Design, 12 (2012) 4995–5001. https://doi.org/10.1021/cg300935k.

[43] P.R. Rout, P. Bhunia, R.R. Dash, A mechanistic approach to evaluate the effectiveness of red soil as a natural adsorbent for phosphate removal from wastewater, Desalination and Water Treatment, 54 (2014) 1–16. https://doi.org/10.1080/19443994.2014.881752.

[44] Y. Kumar, L. Singh, V.S. Sharanagat, A. Patel, K. Kumar, Effect of microwave treatment (low power and varying time) on potato starch: Microstructure, thermo-functional, pasting and rheological properties, International Journal of Biological Macromolecules, 155 (2020) 27–35. https://doi.org/10.1016/j.ijbiomac.2020.03.174.

[45] L.M. Fonseca, J.R. Gonçalves, S.S.M Halal, V.Z. Pinto, A.R.G. Dias, A.C. Jacques, E.R. Zavareze, Oxidation of potato starch with different sodium hypochlorite concentrations and its effect on biodegradable films, LWT - Food Science and Technology, 60 (2015) 714-720. https://doi.org/10.1016/j.lwt.2014.10.052.

[46] L.D. Felix, Kinetic Study of the Discoloration of Crystal Violet Dye in Sodium Hydroxide Medium, Journal of Chemistry and Applied Chemical Engineering, 2 (2018) 1000115. https://doi.org/10.4172/2576-3954.1000115.

[47] Z. Reddad, C. Gerente, Y. Andres, P.L. Cloirec, Adsorption of Several Metal Ions onto a Low-Cost Biosorbent: Kinetic and Equilibrium Studies, Environmental Science & Technology, 36 (2002) 2067–2073. https://doi.org/10.1021/es0102989.

[48] L. Cruz-Lopez, M. Macena, B. Esteves, R. Guiné, Ideal pH for the adsorption of metal ions Cr^{6+}, Ni^{2+}, Pb^{2+} in aqueous solution with different adsorbent materials, Open Agriculture, 6 (2021) 115–123. https://doi.org/10.1515/opag-2021-0225.

[49] R. Foroutan, S.J. Peighambardoust, S.H. Peighambardoust M. Pateiro, J.M. Lorenzo, Adsorption of crystal violet dye using activated carbon of lemon wood and activated carbon/Fe3O4 magnetic nanocomposite from aqueous solutions: A kinetic, equilibrium and thermodynamic study, Molecules, 26 (2021) 348–355. https://doi.org/10.3390/molecules26082241.

[50] L. Jin, W. Li, Q. Xu, Q. Sun, Amino-functionalized nanocrystalline cellulose as an adsorbent for anionic dyes, Cellulose, 22 (2015) 2443–2456. https://doi.org/10.1007/s10570-015-0649-4.

[51] Q. Li. Q. Yue, Y. Su, B. Gao, Equilibrium and a two-stage batch adsorber design for reactive or disperse dye removal to minimize adsorbent amount, Bioresource Technology, 102 (2011) 5290–5296. https://doi.org/10.1016/j.biortech.2010.11.032.

[52] M.A. Haki, A. Imgharn, N. Aarab, A. Hsini, A. Essekri, M. Laabd, H.E. Jazouli, M. Elamine, R. Lakhmiri, A. Albourine, Efficient removal of crystal violet dye from aqueous solutions using sodium hydroxidemodified avocado shells: kinetics and isotherms modeling, Water Science & Technology, 85 (2022) 433–448. https://doi.org/10.2166/wst.2021.451.

[53] L. Baloo, M.H. Isa, N.B. Sapari, A.H. Jagaba, L.J. Wei, S. Yavari, R. Razali, R. Vasu, Adsorptive removal of methylene blue and acidorange 10 dyes from aqueous solutions using oil palm wastes-derived activated carbons, Alexandria Engineering Journal, 60 (2021) 5611–5629. https://doi.org/10.1016/j.aej.2021.04.044.

[54] M.R. Kulkarni, T. Revanth, A. Acharya, P. Bhat, Removal of Crystal Violet dye from aqueous solution using water hyacinth: Equilibrium, kinetics and thermodynamics study, Resource-Efficient Technologies, 3 (2017) 71–77. https://doi.org/10.1016/j.reffit.2017.01.009.

[55] K.M. Mousa, A.H. Taha, Adsorption of Reactive Blue Dye onto Natural and Modified Wheat Straw, Journal of Chemical Engineering & Process Technology, 6 (2015) 1–6. https://doi.org/10.4172/2157-7048.1000260 .

[56] B. Zhang, H. Zhang, Y. Wang, S. Fang, Adsorption behavior and mechanism of amine/quaternary ammonium lignin on tungsten, International Journal of Biological Macrmolecules, 216 (2022) 882–890. https://doi.org/10.1016/j.ijbiomac.2022.07.226.

[57] M. Li, C. Tang, S. Fu, K.C. Tam, Y. Zong, Cellulose-based aerogel beads for efficient adsorption-reduction sequestration of Cr(VI), International Journal of Biological Macrmolecules, 216 (2022) 860–870. https://doi.org/10.1016/j.ijbiomac.2022.07.215.

[58] K.S. Obayomi, M. Auta, A.S. Kovo, Isotherm, kinetic and thermodynamic studies for adsorption of lead(II) onto modified Aloji clay, Desalination and Water Treatment, 181 (2020) 376–384. https://doi.org/10.5004/dwt.2020.25142.

[59] H. Adegoke, F. Adekola, I. Obowookere, A. Yaqub, Thermodynamic studies on Adsorption of lead (II) Ion from Aqueous Solution using Magnetite, Activated Carbon and Composites, Journal Of Applied Science And Environmental Management, 21 (3) 440–452. https://dx.doi.org/10.4314/jasem.v21i3.5.

[60] V. Hernández-Montoya, M.A. Pérez-Cruz, D.I. Mendoza-Castillo, M.R. Moreno-Virgen, A.Bonilla-Petriciolet, Competitive adsorption of dyes and heavy metals on zeolitic structures, Journal of Environmental Management, 116 (2013) 213–221. https://doi.org/10.1016/j.jenvman.2012.12.010.

[61] M. Visa, C. Bogatu, A. Duta, Simultaneous adsorption of dyes and heavy metals from multicomponent solutions using fly ash, Applied Surface Science, 256 (2010) 5486–5491. https://doi.org/10.1016/j.apsusc.2009.12.145.

[62] A. Es-Said, H. Nafai, L.E. Hamdaoui, A. Bouhaouss, R. Bchitou, Adsorptivity and selectivity of heavy metals Cd(II), Cu(II), and Zn(II) toward phosphogypsum, Desalination and Water Treatment, 197 (2020) 291–299.

[63] M.A. Salam, G. Al-Zhrani, S.A. Kosa, Simultaneous removal of copper(II), lead(II), zinc(II) and cadmium(II) from aqueous solutions by multi-walled carbon nanotubes, Comptes Rendus Chimie, 15 (2012) 398–408. https://doi.org/10.1016/j.crci.2012.01.013.

[64] R. Ahmad, K. Ansari, Fabrication of alginate@silver nanoparticles (Alg@AgNPs) bionanocomposite for the sequestration of crystal violet dye from aqueous solution, International Journal of Biological Macromolecules 218 (2022) 157–167. https://doi.org/10.1016/j.ijbiomac.2022.07.092.

[65] A.S. Omer, G.A.E. Naeem, A.I. Abd-Elhamid, O.O.M. Farahat, A.A. El-Bardan, H.M.A. Soliman, A.A. Nayl, Adsorption of crystal violet and methylene blue dyes using a cellulose-based adsorbent from sugercane bagasse: characterization, kinetic and isotherm studies, Journal of Materials research and technology, 19 (2022) 3241–3254. https://doi.org/10.1016/j.jmrt.2022.06.045.

[66] R. Ahmad, A. Mirza, Synthesis of Guar gum/bentonite a novel bionanocomposite: Isotherms, kinetics and thermodynamic studies for the removal of Pb (II) and crystal violet dye, Journal of Molecular Liquids, 249 (2018) 805–814. https://doi.org/10.1016/j.molliq.2017.11.082.

[67] E. Gad, M. Owda, R. Yahia, A Novel Starch Nanoparticle Citrate Based Adsorbent for Removing of Crystal Violet Dye from Aqueous Solution, Egyptian Journal of Chemistry, 63 (2020) 2075–2095. https://doi.org/10.21608/ejchem.2019.16593.2013.

[68] R. Ahmad, K. Ansari, Enhanced sequestration of methylene blue and crystal violet dye onto green synthesis of pectin modified hybrid (Pect/AILP-Kal) nanocomposite,

Process Biochemistry 111 (2021) 132–143. https://doi.org/10.1016/j.procbio.2021.10.009.

[69] H.S. AL-Shehri, E. Almudaifer, A.Q. Alorabi, H.S. Alanazi, A.S. Alkorbi, F.A. Alharthi, Effective adsorption of crystal violet from aqueous solutions with effective adsorbent: equilibrium, mechanism studies and modeling analysis, Environmental Pollutants and Bioavailability, 33 (2021) 214-226. https://doi.org/10.1080/26395940.2021.1960199.

[70] J. Mittal, R. Ahmad, M.O. Ejaz, A. Mariyam, A. Mittal, A novel, eco-friendly bio-nanocomposite (Alg-Cst/Kal) for the adsorptive removal of crystal violet dye from its aqueous solutions, International Journal of Phytoremediation, 24 (2022) 796–807. https://doi.org/10.1080/15226514.2021.1977778.

[71] O.H.P. Gunawardene, C.A. Gunathilake, K.P.S.M. Amaraweera, N.M.L. Fernando, A. Manipura, W.A. Manamperi, K.M.A.K. Kulatunga, S.M. Rajapaksha, A. Gamage, R.S. Dassanayake, B.G.N.D. Weerasekara, P.N.K. Fernando, C.A.N. Fernando, J.A.S.C. Jayasinghe, Removal of Pb(II) Ions from Aqueous Solution Using Modified Starch, Journal of Composites Science, 5 (2021) 1–19. https://doi.org/10.3390/jcs5020046.

[72] R. Ahmad, A. Mirza, Facile one pot green synthesis of Chitosan-Iron oxide (CS-Fe_2O_3) nanocomposite: Removal of Pb(II) and Cd(II) from synthetic and industrial wastewater, Journal of Cleaner Production, 186 (2018) 342–352. https://doi.org/10.1016/j.jclepro.2018.03.075.

[73] Q. Liu, F. Li, H. Lu, M. Li, J. Liu, S. Zhang, Q. Sun, L. Xiong, Enhanced dispersion stability and heavy metal ion adsorption capability of oxidized starch nanoparticles. Food Chemistry, 242 (2017) 256–263. http://dx.doi.org/10.1016/j.foodchem.2017.09.071.

[74] A. Mirza, R. Ahmad, Novel recyclable (Xanthan gum/montmorillonite) bionanocomposite for the removal of Pb (II) from synthetic and industrial wastewater, Environmental Technology & Innovation, 11 (2018) 241–252. https://doi.org/10.1016/j.eti.2018.06.009.

[75] J. Mittal, R. Ahmad, A. Mariyam, V.K. Gupta, A. Mittal, Expeditious and enhanced sequestration of heavy metal ions from aqueous environment by papaya peel carbon: a green and low-cost adsorbent, Desalination and Water Treatment, 210 (2021) 365–376. https://doi.org/10.5004/dwt.2021.26562.

Authors contribution

Conceptualization [Katarina Trivunac] and [Marija Vukčević]; Material preparation and investigation [Nataša Karić], [Marina Maletić], and [Silvana Dimitrijević]; Data analysis and Writing-original draft [Nataša Karić], [Marija Vukčević], [Marina Maletić], and [Katarina Trivunac]; Writing – review & editing the paper [Mirjana Ristić] and [Aleksandra Perić Grujić]. All authors read and approved the final manuscript.

Declaration of interests

In my personal name and on behalf of all coauthors of this research, as the corresponding author of this publication, I declare under full responsibility, that there are NO known competing financial interests or personal relationships that could have appeared to influence the work reported in this paper.

The first and corresponding author, Nataša Karić

Graphical abstract

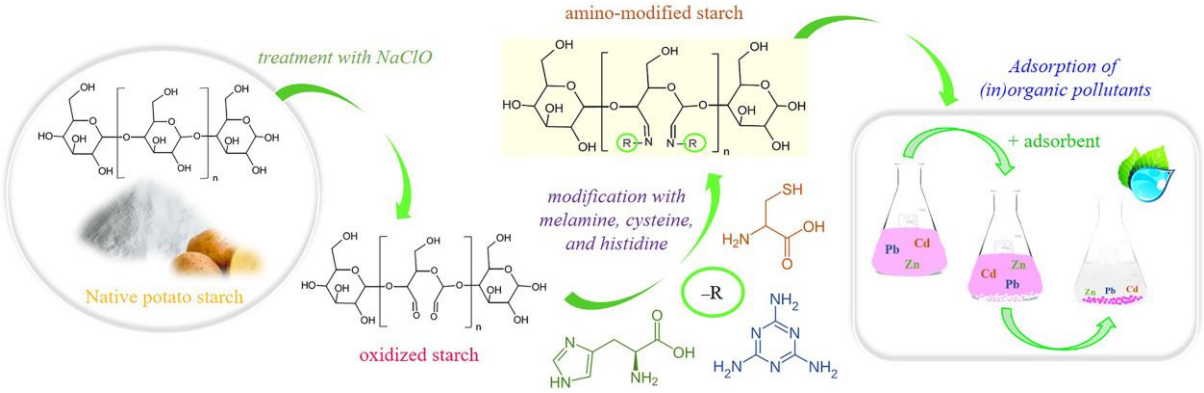

Highlights

- Natural macromolecule, starch, as a cheap and effective adsorbent for dyes and heavy metals
- Efficient and eco-friendly process for starch modification with melamine and amino acids
- The materials proved to be the most effective in removing crystal violet and Pb^{2+}
- Amino-modified starch with histidine proved to be the most effective adsorbent